Final report on prospective sites for the geological storage of CO_2 in the southern Baltic Sea

Appendix A Dynamic modelling

Elforsk report 14:54

SLR Consulting & Uppsala university

March 2014

ELFORSK

Final report on prospective sites for the geological storage of CO_2 in the southern Baltic Sea

Appendix A Dynamic modelling

Elforsk report 14:54

SLR Consulting & Uppsala university

March 2014

Appendix A - Modelling of CO_2 spreading and related pressure response in Dalders Monocline and Dalders Structure – Uppsala University, Department of Earth Sciences

16.0 MODELING OF CO_2 SPREADING AND RELATED PRESSURE RESPONSE IN DALDERS MONOCLINE AND DALDERS STRUCTURE

Auli Niemi, Zhibing Yang, Liang Tian, Byeongju Jung, Fritjof Fagerlund, Saba Joodaki

Uppsala University, Department of Earth Sciences

We have carried out preliminary modeling of CO_2 injection into selected parts of the Dalders Monocline and Dalders structure, in order to estimate the feasibility of these formations for industrial scale CO_2 injection. This Appendix presents the results of this study, this Chapter 16 presents the summary of the results and Chapters 17 to 21 present the underlying work.

The approach taken in the modeling has been to use different modeling approaches parallel, thereby increasing the confidence and reliability of the predictions, given the data available at the present moment. The modeling approaches used are 1) preliminary determination of the injection rates by means of analytical solution; 2) Numerical modeling of CO_2 plume spreading and related effects effects with TOUGH2 model and 3) vertical- equilibrium (VE) model. We have also estimated the long-term CO2 transport by means of analytical and TOUGH2 models. The objective of this preliminary study is to get order-of-magnitude estimates of the behavior of the formations during the CO_2 injection and subsequent storage periods under specific injection scenarios. Below we will first discuss the results of the major formation, the Dalders Monocline and then proceed to the considerably smaller formation, the Dalders Structure. In the case of the Dalders Monocline, the focus is in the southern part of this domain (see Figure 4 in Part B) where there is high confidence in the characteristics of the overlying cap-rock.

The data and static geological models for these simulations have been provided by SLR and are presented elsewhere in this report. For the numerical models (TOUGH and VE models) the permeability and porosity maps presented in the static model were directly used (Figures 13 a and b) as input and for the analytical models single homogeneous values were used and varied within the realistic range.

16.1 Dalders Monocline

The target area modeled for the CO_2 injection is the deep (southernmost) part of the Dalders Monocline. The modeled units are the lower and middle Cambrian units, which have relatively high permeability and porosity, and are mostly continuous within the monocline area. From above the aquifer is sealed by thick Ordovician units and Alum shale that can work as excellent cap-rocks. The thickness of Cambrian units varies depending on locations, but generally the structure become thinner and pinches out by moving northward. The overall thickness in the deepest part is about 100 m. The southern side of the monocline is bounded by a fault zone, and the sedimentary units

in the northern side are exposed in the submarine/atmosphere. We assume the southern boundary of the modeling domain to be closed (but a sensitivity study considers an open condition here as well) and the northern boundary to be open. The hydrogeological parameters used in the model were obtained from several boreholes spread over the monocline.

As the first model (Part A) we use an analytical solution by Mathias et al. (2011a,b), to get an initial estimate of what CO_2 injection rates can be used, in order not to cause pressure increases resulting in unacceptable mechanical effects. As site-specific mechanical information is presently lacking, we use a commonly applied estimate of 1.5 times the initial hydrostatic pressure as a preliminary pressure cutoff criterion. The analytical model assumes homogeneous and uniform medium properties. It takes into account the injection well interference with other wells. Using the mean values of the formation as the base case, and assigning a maximum allowed pressure of 180 bars, then the maximum injection rate is about 0.5 Mt/yr per well when injecting simultaneously from five wells for fifty years. This would correspond to 2.5 Mt/yr in total for five wells and the area considered is the southern part of the Dalders Monocline. Figures 1 to 3 of Part A allow inspecting how varying different factors, such as layer thickness and permeability, influences the maximum allowable injection rate. Figure 3 also shows the effect of the number of injection wells, where it can be seen that distribution of the injection to a larger number of wells reduces the injection pressure.

The base-case result of 0.5 Mt/year per well was used as a starting point in the subsequent numerical simulations, where numerical simulations with TOUGH2 and TOUGHMP (PART B) and VE-models (PART E) were used for more detailed analyses. With these numerical models the local variations in material properties, thickness etc., as well as processes like CO_2 dissolution can also be taken into account.

The TOUGH2 simulations (PART B) were carried out by gradually increasing the complexity of the model, starting from coarse 2D models (or 'pseudo 3D' models where layer thickness was varied while keeping the model 2D) and proceeding to finer discretization and fully 3D models (Table 2 of Part B). Also here the focus is on the southern part of the Dalders Monocline. The most interesting results are those from the full 3D cases (Cases 4 and 5) where fine discretization was used near the injection wells and the domain was vertically discretized, to allow a realistic interpretation of the buoyancy flow. In the single well injection case, where 0.5 Mt/year is injected in the centrally located well (inj_02; Figure 4, Part B) the maximum overpressure is about 60% (Figure 12). The plume spreading (in the uppermost layer where the spreading has reached farthest, due to buoyancy, see Figure 11) can be seen in Figure 13, from which it can be seen that the spread of the plume is about 7 km at the end of the 50 years injection. After the end of the injection, when the injection pressure driving force is removed the plume advancement is slow and after 158 years (Figure 14) the plume still has moved to less than 8 km from the injection well.

In the case of the multiple well injection, where 0.5 Mt/yr was injected from the middle and eastern wells and 0.2 Mt/yr from the southernmost well situated in the vicinity of the closed lower boundary (Figure 4, PART B). A smaller injection rate was used in the southernmost well as the results from the VE-model (Part D) had shown unacceptably high pressure increases in case the 0.5 Mt/yr rate was used from this well also. In this case the plume spreading pattern is similar to that in the Case

4 single-well injection, and even the maximum pressure increase in the well where results could be compared (central well, Figure 16). Also in this case the highest overpressure in the central injection well was of the order of 60% (as in the single well scenario), which is also in good agreement with the analytical solution of PART A. In the southernmost well close to fault zone the pressure increases were higher, as can be expected.

The vertical equilibrium model is a simplified, yet powerful approach used quite extensively in large scale modeling predictions of CO_2 injection. It is especially used in the academia and considered as one of the main alternative approaches for full 3D numerical simulations. The results (Figure 6, Part D) are in good agreement with TOUGH simulations in terms of the spreading of the CO_2 plume. The extent of the plume is less that 10 km at the end of the injection and the movement after the end of injection slow. It should be noted that here the plume of certain thickness is shown, not the CO_2 saturation like in the case of TOUGH2 simulations. The predicted pressure distribution also matches well with the results from other methods, with overpressures of about 90% at injection wells (A and C) in case of 0.5 Mt/year injection per well for 50 years (Figure 5, Part D). The higher pressure in the multiple-well scenario can be partly explained by the extreme pressure response at the southernmost well (Well B in Figure 5, Part D) that is very close to the fault zone.

Finally, the CO_2 migration time after the end of the injection is considered in Part E. Also here the TOUGH2 simulations are used as the simulation method. Assuming the prevailing formation slope and other best estimate properties, the plume migration distance as function of the time for two different permeabilities can be seen in Figure 8. Figure 9 shows the effect of residual saturation on this distance. The results indicate that it would take for the tip 4000 years to travel 14 km. If we consider a total amount of 30 Mt injected CO_2 for one injection well, with Sgr= 0.2, a simple volumetric calculation may yield a potential maximum migration distance of about 50 km, taking into account the plume shape and equilibrium dissolution within the plume. According to the average speed of migration (Figure 9, Part E) a migration distance of 50 km would take about 14000 years. Given this distance and the especially long time, we can also calculate the dissolution trapping capacity. The mass that can potentially be dissolved in our considered system can be estimated to half of the initial CO_2 mass. This means that, in this case, convective dissolution has the potential to significantly drag the plume migration, and that the plume migration distance will be actually much smaller than 50 km in 14 000 years. This can be compared to the 120 km distance between the point of injection and Gotland Island.

16.2 Dalders Structure

This much smaller area is an anticline structure attached to the southern part of the Dalders monocline, consisting of Cambrian sedimentary units. Thick low-permeable Ordovician sequences and shale layers provide a good sealing capacity. The depth ranges 1.3 ~ 1.4 km below sea level, and the physiographic map shows three high locations suitable for commercial size CO_2 injection operation. The northern boundary of the structure is a closed fault zone and considered a closed

boundary in these simulations. The southern boundary is a spill point, and assumed as an open boundary.

The location of the injection well was chosen in the middle of the structure where the depth is relatively deep; hence we can easily observe the overpressure development and migration induced by the CO_2 injection. The injection rate and period applied to one well (Figure 1, Part C and Figure 9, Part D) are 0.3 Mt/year and 0.5 Mt/yrs for 50 years for TOUGH2 model and 0.3 Mt/year for 50 years for the VE-model. With the TOUGH2 model the vertical layering was taken into account (Figure 1, Part C) while with the VE-model the layering was ignored due to the character of the model. With the TOUGH2 model both the 0.3 Mt and 0.5Mt injection scenarios showed moderate pressure increase of less than 50% compared to the in-situ hydro-equilibrium pressure (Figure 2, Part C). Similar pressure increases were observed with the VE-model (Figure 10, Part D).

Based on the TOUGH simulations low CO_2 saturations reach the model boundaries prior to end of injection, which is obviously not desirable. Estimates of this leakage are also given. Similar plume spreading is observed with the VE-model but as here the CO_2 thickness is given rather than CO_2 saturations, the effect of reaching the model boundaries is not as obvious from the Figures. After the end of the injection the plume is migrating up-dip and getting diluted, due to residual trapping and dissolution. These preliminary results indicate that while the pressure increase induced by the injection is acceptable, the location of the well(s) should receive more attention or more detailed calculations to address the question of the plume reaching model boundaries prior to the end of the 50 years injection.

16.3 Concluding remarks

To summarize, the preliminary modeling presented here indicates for the southern part of the Dalders Monocline a maximum total injection rate of the order of 2.5 Mt/yr, assuming a maximum sustainable pressure increase of 50% from the hydrostatic condition, injection from five wells and a homogeneous permeability of 40mD with layer thickness of 50m. This maximum injection rate is sensitive to parameters such as formation thickness, permeability as well as number of wells. Sensitivities to these parameters are shown in Figures 1 to 3 in Chapter 17, indicating how increasing the number of wells would allow a larger total injection rate and how an increase/decrease in permeability influences the maximum injection rate. Reducing the total injection time from 50 years to e.g. 25 years, would also allow increasing the injection rate, as the pressure increase due to injection increases with time. The above results come from the preliminary analytical models but are supported by the results from the numerical models.

In these preliminary simulations the model parameters were taken from the static model as such. For the numerical models the properties were spatially varying while for the analytical models single homogeneous values were used and varied within the realistic range. It should be pointed out that in future studies more comprehensive sensitivity and uncertainty analyses could and should be carried out to test the sensitivity of the numerical models to uncertainties in the input parameter values.

It should also be pointed out that in these preliminary simulations we have assumed impermeable sealing units for the storage formation. The injection-induced pore pressure could be dissipated by brine displacement through cap-rock (pressure ‘bleed-off’) if the permeability of the cap-rock is not extremely low and the compressibility of the cap-rock is large (see e.g., Chang et al. 2013). In addition, pore pressure could be further relieved through brine production wells. The role of using horizontal, rather than vertical injection wells could also be investigated. Finally it should be noted that the assumed 50% sustainable pressure increase is a reasonable assumed value based on literature, as site-specific mechanical information is presently lacking. Further studies should address these issues in more detail. Such analyses should also be accompanied with additional site-specific data.

Finally, it should be pointed out that in future studies more detailed models describing the behavior near the borehole could be used, including simulators with specific wellbore modules that allow detailed gridding near the borehole.

PART A

17.0 PRELIMINARY DETERMINATION OF MAXIMUM INJECTION RATE BY MEANS OF ANALYTICAL SOLUTION

Zhibing Yang, Auli Niemi

17.1 Introduction

Effective implementation of CO_2 sequestration involves injection of large volumes of CO_2 which causes pressure perturbation in the storage formations. The increase in pore pressure due to injection induces changes in the stress field. This generally increases the risk of shear and tensile failure (which jeopardizes the integrity of the storage reservoir) as well as reactivation of pre-existing faults. In this part of the work, we evaluate the injection induced pore overpressure for the Dalders Monocline via the state of the art analytical model developed for CO_2 storage by Mathias et al. (2011a, b). We investigate the dependence of the formation pressure buildup on the CO_2 injection rate for different parameters such as layer thickness, permeability, number of injection wells. This can be used to preliminarily determine the maximum injection rate if a maximum allowable pressure increase is given.

17.2 Modeling approach

In this section, we briefly introduce the analytical solution developed by Mathias et al. (2011a, b). Under reservoir conditions, supercritical CO_2 can partially dissolve into brine and at the same time water can partially vaporize in the presence of CO_2. This partial miscibility gives rise to complex flow regimes and dynamics for the evaluation of pressure response. For a typical industrial-scale CO_2 injection scenario, there exist a dry-out zone (free of water) around the injection well. In this dry-out zone all water has been either displaced outwards or vaporized into the CO_2 rich (gas) phase and the salt that was originally dissolved in the brine has precipitated. The radius of dry-out zone is typically on the scale of 10^2 meters at the end of the injection period (say e.g. 50 years). Surrounding the dry-out zone is a region where the gas phase and the aqueous phase coexist. The radius of this two-phase flow region is typically several kilometers at the end of the injection period. Outside of the two-phase region only brine exists with single phase brine flow. Assuming vertical pressure equilibrium, constant fluid properties, negligible capillary pressure and equilibrium dissolution between CO_2 and water, Mathias et al. (2011b) solved the relevant (radially symmetric) governing equations describing the above flow characteristics. It is possible to obtain closed-form solutions for the gas saturation and pressure for the case with linear relative permeability functions.

For nonlinear relative permeability functions, numerical evaluation of the gas saturation at the leading shock front needs to be used, and the solution becomes semi-analytical.

The analytical model of Mathias et al. (2011b) can be applied to both open and closed aquifers. It can be summarized as:

$$\Delta P = P - P_{ini} = \frac{M_0}{4\pi\rho_g Hk}\begin{cases}\mu_g q_{D1}\ln(z_T/z)/k_{rs} + \mu_g q_{D2}F_2(z_T) + \mu_b q_{D3}F_1(z_L), & 0 \le z < z_T \\ \mu_g q_{D2}F_2(z) + \mu_b q_{D3}F_1(z_L), & z_T \le z < z_L \\ \mu_b q_{D3}F_1(z), & z \ge z_L\end{cases} \quad (1)$$

where ΔP is the pressure build-up,

P is the vertically averaged pressure,

P_{ini} is the initial pressure (vertically averaged),

M_0 is the mass injection rate of CO_2,

ρ_g is the density of CO_2,

μ_g is the viscosity of CO_2,

k is the permeability of the formation,

H is the thickness of the formation,

k_{rs} is the permeability reduction factor due to salt precipitation,

μ_b is the viscosity of the brine,

q_{D1}, q_{D2}, and q_{D3} are the dimensionless, piecewise total fluxes, which can be obtained from Equations (27) and (28) in Mathias et al. (2011b),

z is the similarity transform variable for time t and radial distance r

$$z = \frac{\pi\phi\rho_g Hr^2}{M_0 t},$$

and z_T and z_L are locations of the trailing and leading shocks in similarity space, which can be evaluated from Equations (30-35 and 53) in Mathias et al. (2011b).

In Equation (1),

$$F_1(z) = \begin{cases}(\alpha z_E)^{-1} - \frac{3}{2} + \ln\left(\frac{z_E}{z}\right) + \frac{z - z_L}{z_E}, & z_E < \frac{0.5615}{\alpha} \\ E_1(\alpha z), & z_E > 0.5615/\alpha\end{cases}$$

with $\alpha = \dfrac{M_0 \mu_b (c_r + c_b)}{4\pi \rho_g H k}$,

$$F_2(z) = -\frac{1}{\mu_g} \int_z^{z_L} \left(\frac{k_{ra}}{\mu_b} + \frac{k_{rg}}{\mu_g} \right)^{-1} \frac{1}{z} dz$$

where ρ_b is the density of the native brine,

ϕ is the porosity,

z_E is similarity transform for the radial extent of the formation r_E,

k_{ra} and k_{rg} are the relative permeabilities of the aqueous phase and gas phase, respectively,

and c_r and c_b are the compressibilities of rock and brine, respectively.

For more details of the analytical model, see Mathias et al. (2011b).

17.3 Modeling scenario and parameters

We perform modeling for a domain consisting of the southern part of the Dalder Monocline. The modeling domain covers an area of about 22260 km^2 (see Figure 3 and 4 in PART B for maps). The storage formation is idealized into a layer with uniform thickness and homogeneous permeability and porosity. The domain is bounded by faults in the south (boundary AC in Figure 4 in PART B) which may be considered as impermeable. The other boundaries can be considered open. The overlying and underlying formations are assumed to be impermeable. Since we are considering multiple injection wells distributed over the modeling domain, the pressure perturbation from each well will interfere with that from the surrounding wells. As a result, the wells that are not close to the open domain boundaries will effectively behave as if they were surrounded by a no-flow boundary. Therefore, in the modeling of pressure buildup in the vicinity of the injection well, we consider a closed domain for each individual injection point with domain radial extent r_E determined by the domain area A and the number of injection wells n_w, that is, $r_E=(A/2\pi n_w)^{0.5}$.

Base case parameters used for the pressure analysis are given in Table 1 (based on the averaged values of property maps given by SLR for the Dalders Monocline). The fluid properties depend on the pressure and thus cannot be known beforehand. Therefore, we use iterative procedures to find the pressure and at the same time the fluid properties such as densities, viscosities, dissolved mass fractions of CO_2 in water and water in CO_2.

Table 1. Base-case modeling parameters for pressure buildup at the injection wells.

Parameter	Value and unit
Initial pressure P_{ini}	120 bars
Number of wells n_w	5
Permeability k	40 mD
Thickness H	50 m
Porosity φ	0.12
Injection time t	50 years
Rock compressibility c_r	4.5×10^{-10} Pa^{-1}
Brine compressibility c_b	3.54×10^{-10} Pa^{-1}

17.4 Estimation for maximum injection rates

We model the pore pressure at the injection well for a series of injection rates. Sensitivity of the injection rate – pressure dependence to the modeling parameters is explored for formation thickness, permeability and number of wells.

Results (Figure 1-3) suggest that pore pressure (and thus pressure buildup) increases approximately linearly with injection rates. They also show that the pore pressure increase is very sensitive to the chosen parameters (formation thickness, permeability and number of wells).

In order to estimate the maximum injection rates, we need to know the sustainable pressure buildup that a given storage system is expected to tolerate without geomechanical degradation (such as microfracturing and/or fault reactivation) for the sealing structures (Rutqvist et al., 2007; Zhou et al., 2008). However, the sustainable pressure buildup should be obtained on a site-by-site basis since it is depending on the in situ stress field and the geomechanical properties of the rock units. Due to the lack of detailed measurements of geomechanical properties of the sealing structure and in situ stress condition in our case here, we assign a maximum pressure increase of 50% from the initial hydrostatic pressure. This corresponds to a maximum pore pressure of 180 bars (or maximum pressure buildup of 60 bars) close to the injection well. The threshold pressure increase of 50% is in accordance with Zhou et al. (2008). We note that the sustainable pressure buildup should be reevaluated once site-specific information on in situ stress and geomechanical properties is obtained.

According to the base case result (the green curves in the following figures), if we assign a threshold pore pressure of 180 bars, then the maximum injection rate is about 0.5 Mt/yr per well. This would correspond to 2.5 Mt/yr in total for five wells.

Figure 1 shows how decreasing/increasing layer thickness influences the maximum injection rate (e.g., increasing the thickness from 50 m to 60 m would increase the injection rate per well to about 0.7 Mt/year). Figure 2 in turn shows the large effect of formation permeability. For example, increasing the permeability to 80 mD would increase the allowed injection rate to over 0.8 Mt/year. Finally, Figure 3 shows the effect of number of injection wells, where it is clear that distribution of the injection to a larger number of wells reduces the injection pressure.

The base-case result of 0.5 Mt/year was used as starting point in the subsequent numerical simulations (PART B and D) with TOUGH2 and VE-models, where local variations in material properties, thickness etc., time-dependent behavior and variable boundary conditions could be taken into account more accurately.

17.5 Discussion

We have performed analytical modeling of pressure buildup for the southern part of the Dalders Monocline using a recently developed semi-analytical solution. For the base-case parameters we obtained a maximum total injection rate of 2.5 Mt/yr, assuming a maximum sustainable pressure increase of 50% from the hydrostatic condition. Sensitivity study results indicate that the maximum injection rate can be sensitive to parameters such as formation thickness, permeability and number of wells.

It is worth noting that the 2.5 Mt/yr (multiplied by 50 years) should not be directly used for pressure-limited capacity estimation. In our case here, we have assumed impermeable sealing units for the storage formation. The injection-induce pore pressure could be dissipated by brine displacement through caprock if the permeability of the caprock is not extremely low and the compressibility of the caprock is large (see e.g., Chang et al. 2013). In addition, pore pressure could be further relieved through brine production wells. However, the technical and economic feasibility should be evaluated for this option.

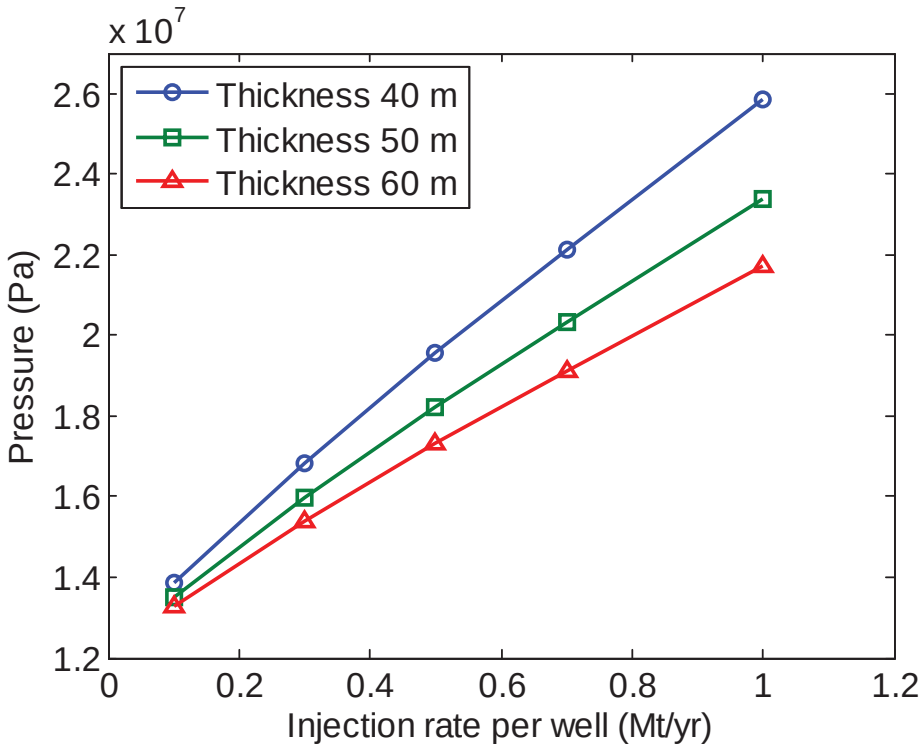

Figure 1. Sensitivity of injection pressure to injection rate for different layer thicknesses.

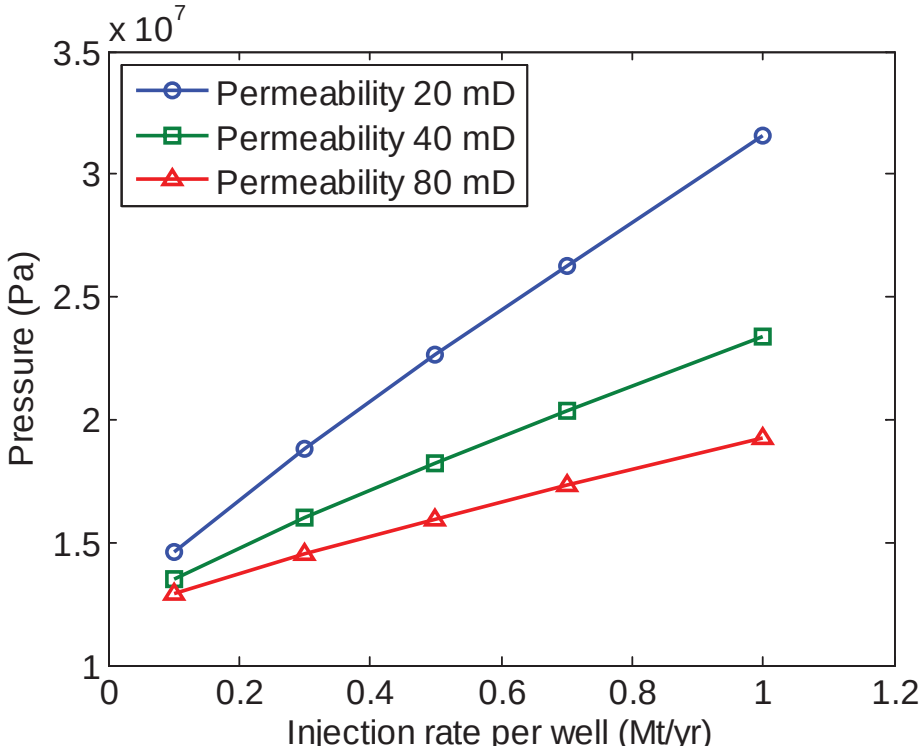

Figure 2. Sensitivity of injection pressure to injection rate for different layer permeabilities. Injection pressure is very sensitive to formation permeability.

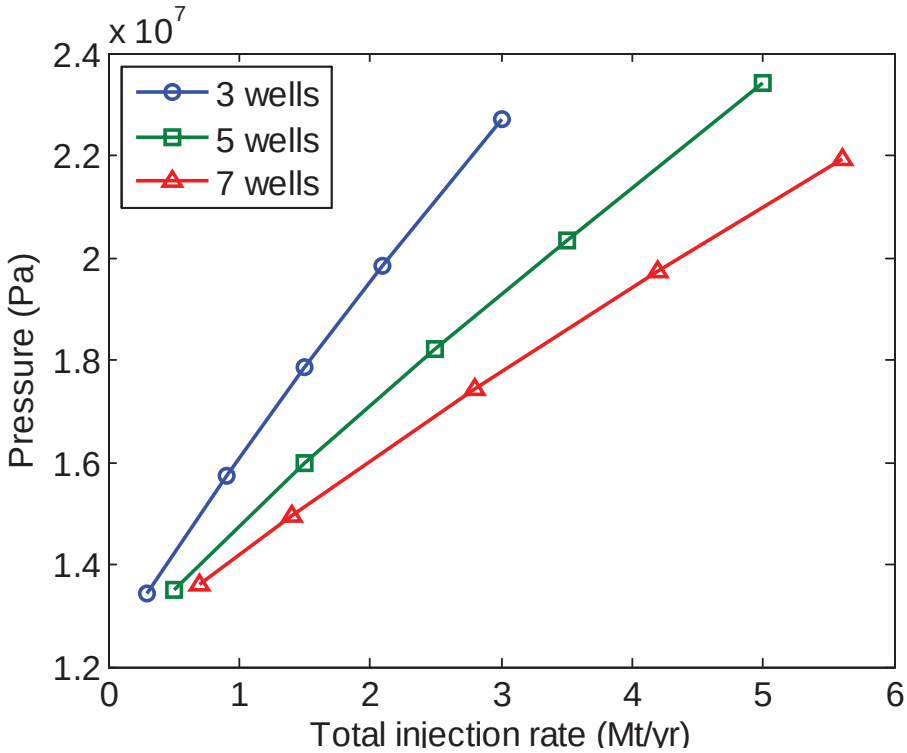

Figure 3. Sensitivity of injection pressure to injection rate for different number of wells.

17.6 References

Chang KW, Hesse MA, & Nicot JP (2013) Reduction of lateral pressure propagation due to dissipation into ambient mudrocks during geological carbon dioxide storage. *Water Resour. Res.* **49**, 2573-2588, doi:10.1002/wrcr.20197.

Mathias SA, González Martínez de Miguel GJ, Thatcher KE, & Zimmerman RW (2011a) Pressure buildup during CO_2 injection into a closed brine aquifer. *Transport in Porous Media* **89**, 383–97.

Mathias SA, Gluyas JG, González Martínez de Miguel GJ, & Hosseini SA (2011b) Role of partial miscibility on pressure buildup due to constant rate injection of CO_2 into closed and open brine aquifers. *Water Resources Research* **47**, W12525.

Rutqvist J, Birkholzer JT, Cappa F, & Tsang CF (2007) Estimating maximum sustainable injection pressure during geological sequestration of CO_2 using coupled fluid flow and geomechanical fault-slip analysis. *Energy Convers. Manag.* **48**, 1798–1807, doi:10.1016/j.enconman.2007.01.021.

Zhou Q, Birkholzer JT, Tsang CF, and Rutqvist J (2008) A method for quick assessment of CO_2 storage capacity in closed and semi-closed saline formations, *Int. J. Greenh. Gas Control*, **2**, 626–639, doi:10.1016/j.ijggc.2008.02.004.

PART B

18.0 SIMULATION OF CO2 SPREADING AND RELATED PROCESSES WITH TOUGH2 MODEL – DALDERS MONOCLINE

Liang Tian, Fritjof Fagerlund and Auli Niemi

18.1 Dalders Monocline - Model description

18.1.1 Digital elevation model (DEM) and SLRs static model

The modeled region is centered at the Baltic Sea basin (Figure1). The subsurface topography is described by 1000 m grid Digital Elevation Model (DEM). A three- dimensional geological structure model is constructed for an area of dimensions 549 km x 369 km among which the Dalders Monocline static model is mapped covering an area of 72,168 km^2. Table 1 summarizes the geo-hydrological properties of the static model. All the information concerning the static model and related parameter values for this modeling work have been obtained from SLR.

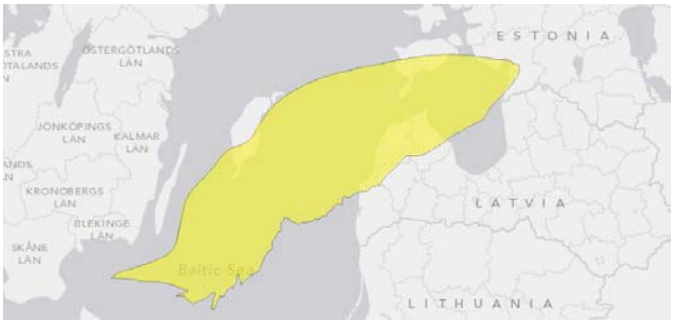

Figure 1. Map view of the modeling region highlighting the Mid-Cambrian (Dalders Monocline)

Table 1. Summary of the geo-hydrological properties mapping from the static model

Data Resolution	1000m		
Porosity	4,30%	-	20,60%
permeability	8,5 mD	-	300 mD
formation top	-225 m	-	-1756 m
Thickness	0 m#	-	82 m

#note: the formation pinches out at the edge of the reservoir which results in zero thickness.

18.1.2 Conceptual model and numerical grid

For the purpose of numerical modeling with the TOUGH2 code (Pruess, 1999) several conceptual models and numerical grids were considered. The first coarse model considered the entire region of interest and was a 'psuedo-3D' model consisting of one layer of variable thickness in the vertical direction, and a 2D plane with uniform size grid blocks of dimension 5000 x 6000 m (Figure 2). The permeability, porosity, top and bottom elevations were retained by linear interpolation from the information provided by SLR. No vertical discretization was included in this first model. As can be seen in Figure 2, the formation is deepest in the South-Eastern part and gradually becomes thinner and shallower towards North-West.

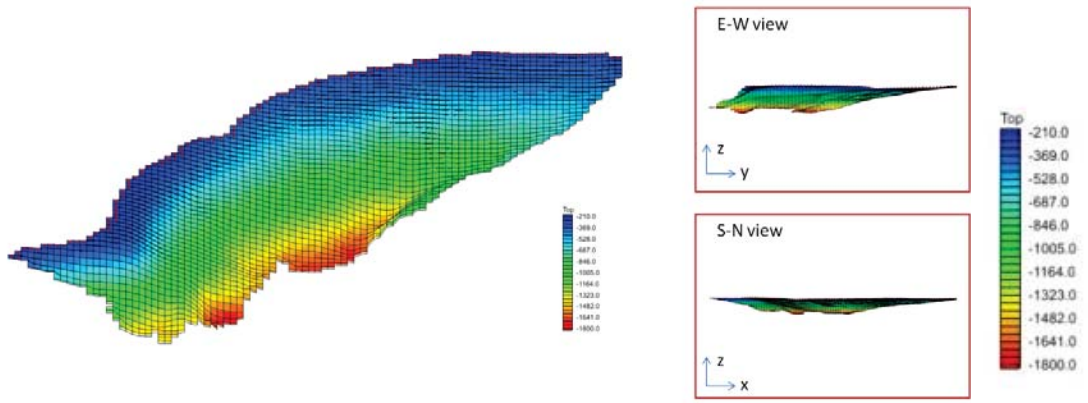

Figure 2. Coarse model for the Dalders Monocline - the color indicates the elevation of the formation top (from the mean sea level in units of m).

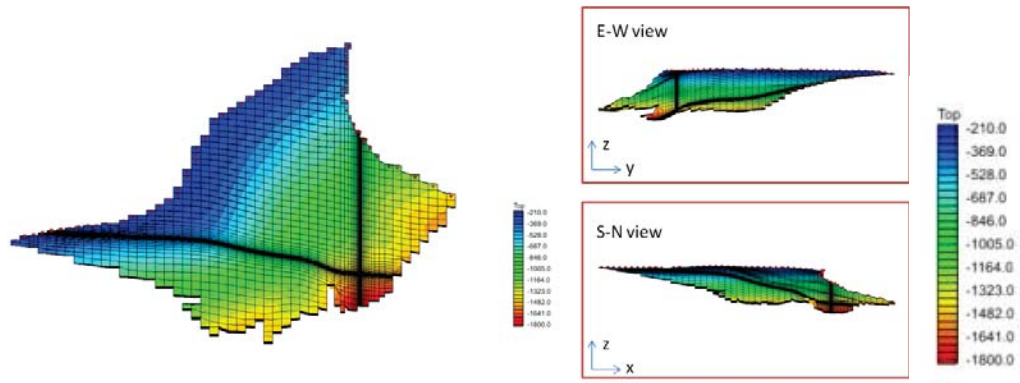

Figure 3. Model for the Southern Dalders Monocline - the color indicates the elevation of the formation top (from the mean sea level in units of m). Finer discretization in the vicinity of the injection well.

A second model was created focusing only on the southern half of the Dalders Monocline static model where the cap-rock integrity is most confidently identified. In this model also a more refined grid is used in the vicinity of the injection well, by using a gradual refinement method. For this second domain both 'pseudo-3D' and a full 3D models were considered. In the full 3D case the model was vertically discretized into 7 element layers. As insufficient information was available concerning the local heterogeneity in the vertical direction, permeability and porosity were assumed vertically homogeneous. No permeability anisotropy was considered. The vertical discretization does still allow a more realistic evaluation of the buoyancy flow of the upwards migrating CO_2.

An example discretization of the model for the southern part is shown Figure 3. In this example only one injection well is shown. All the simulation scenarios considered will be summarized in detail in section 1.4.

18.1.3 Initial and boundary conditions

The initial condition for pressure is obtained by assuming a gravity equilibrium condition. Salinity is assumed constant in the entire modeling domain and to be 11.54% (wt. NaCl based on data from well E7-1). Due to lack of thermal information, isothermal condition is considered with a constant temperature of 50°C.

In these simulations the overlying cap-rock is assumed impermeable and closed boundary conditions are used both at the top and bottom of the modeling domain. For the lateral boundaries the following boundary conditions are used (Figure 4.): in the north-east and north (A-B'-B) the boundary is open (constant pressure boundary), in the south and south-east side (A-C-B), there is uncertainty in the character of the boundary condition and therefore both open and closed conditions are considered. When focusing only at the southern Dalders Monocline the east side boundary (B'-C) is set open, allowing fluid to enter the north-eastern part of the formation.

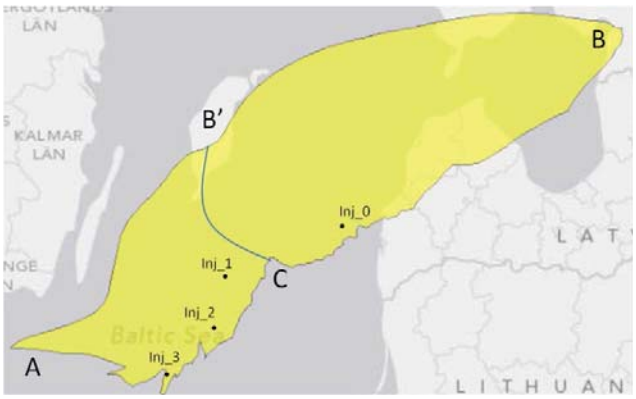

Figure 4. Boundary condition locations and locations of the injection wells.

The injection of CO_2 takes place through one or several vertical injection wells. The locations of the injection wells are presented in Figure 4 as well. The injection rate was initially determined by the semi-analytical calculations presented in Part A. The supercritical CO_2 is injected continuously for 50 years. Then the post-injection development is monitored for 950 years. The total simulation covers 1000 years.

18.1.4 Model Scenarios

The model scenarios are summarized in Table 2.

Table 2. Model scenarios

Case	Model domain	Conceptual Model	Boundary conditions		Injection Rate ($MtCO_2$/year)			
			A-B'-B (A-B')	A-C-B(A-C)	inj_0	inj_1	inj_2	inj_3
1	Dalders Monocline	Psuedo 3D	Open	Closed	3,0	-	-	-
2	Southern Dalders Monocline (Case 2-5)	Psuedo 3D	Open	Closed	-	-	1,0	-
3		Psuedo 3D	Open	Open	-	-	1,0	-
4		3D	Open	Closed	-	-	0.5	-
5		3D	Open	Closed	-	0,5	0,5	0,2

The purpose of Case 1 is to obtain a first estimate of the general CO_2 migration pattern. Cases 2 to 4 are designed to test specific assumptions, namely boundary conditions and the effect of vertical discretization. Case 5 is designed to test a specific injection strategy of three wells instead of one well, like in the other cases.

18.2 Numerical Simulations

TOUGH2/ECO2N simulator is used to simulate the migration of CO_2 in the formation. (Pruess et.al, 1999; Pruess, 2005) TOUGH2MP, a massive parallel version of TOUGH2 is used for the more computational demanding 3D simulations. (Zhang et.al, 2008). The two-phase flow characteristic functions are the van Genuchten model (van Genuchten, 1980) for the capillary pressure–saturation function and the van Genuchten–Mualem model (Mualem, 1976; van Genuchten, 1980) for the relative permeability functions. To simulate the CO_2-brine two-phase flow in the heterogeneous medium, the Leverett scaling (Leverett, 1941) is applied, i.e. capillary entry pressure (P_c) is scaled in relation to the permeability according to

$$P_c = P_{c,ref}\sqrt{\frac{k_{ref}}{k}}$$

The parameters used for the simulations are listed in Table 3. These parameters are chosen as typical literature values due to a lack of relevant data. They fall into the range of parameters used by, for example, Doughty (2007) and Zhou et al. (2010). The choice of parameters will have an impact on the simulation results. For overpressure estimation, the impact of capillary pressure would be negligibly small (Mathias et al., 2011), while the relative permeability parameters may have a sensible effect. However, the uncertainty in estimating overpressure due to unknown relative permeability parameters will likely be less significant than that resulted from other parameters such as permeability, porosity etc. Nevertheless, it would be beneficial for modeling if more field data and core measurements especially regarding two-phase flow properties can be obtained in the future.

Table 3. Parameters used in the simulations

Parameters	*Values*
Irreducible water saturation, $S_{l,r}$ [-]	0.300
Residual gas saturation, $S_{g,r}$ [-]	0.050
Van-Genuchten parameter, m [-]	0.457
Reference for Leverett scaling on capillary pressure, P_{ref} [Pa]	1.98×10^{4}
Reference permeability, k_{ref} [mD]	100
Pore compressibility [Pa^{-1}]	$4.5\text{x}10^{-10}$

The Ground Water Modeling system (GMS, Aquaveo, LLC) is used to create the integral finite difference method grids. A modified version of TMT2 (Borgia et.al, 2011) is used to convert the Modflow 2000 grid to TOUGH2 format. The grid block information is summarized in Table 4.

Table 4. Numerical grids used in the different cases

	Modeling Domain	Vertical Section(s)	Grid refinement			Number of grid elemets	Case
			Min (m)	Max (m)	Bias		
1	Dalders Monocline	1	-	-	-	7 154	1
2	Dalders Monocline Southern	1	10	5000	1.1	4 968	2,3
3	Dalders Monocline Southern	7	10	5000	1.1	34 776	4
4	Dalders Monocline Southern	7	50	5000	1.3	73 794	5

18.3 Results and discussion

18.3.1 Case 1

A coarse grid is used for a preliminary injection simulation run with an injection rate of 3MtCO_2 / year. To be able to describe the pressure build up, an overpressure factor (F_{op}) is defined as

$$F_{op} = (P - P_{hydro\text{-}initial}) / P_{hydro\text{-}initial} \times 100\%$$

where the P is the injection pressure during the simulation run and $P_{hydro\text{-}initial}$ is the initial pressure.

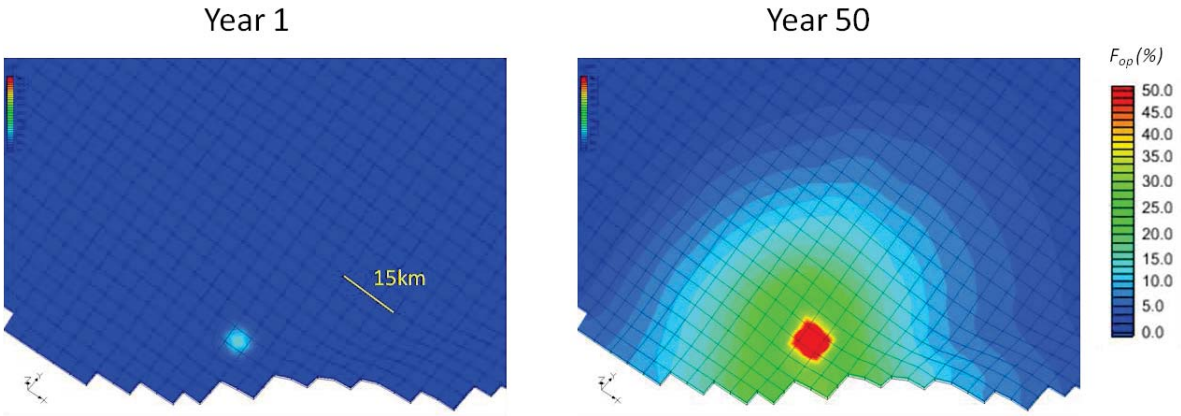

Figure 5. Case 1 - The over pressure factor F_{op} shows the pressure build up at year 1 and year 50 (end of injection).

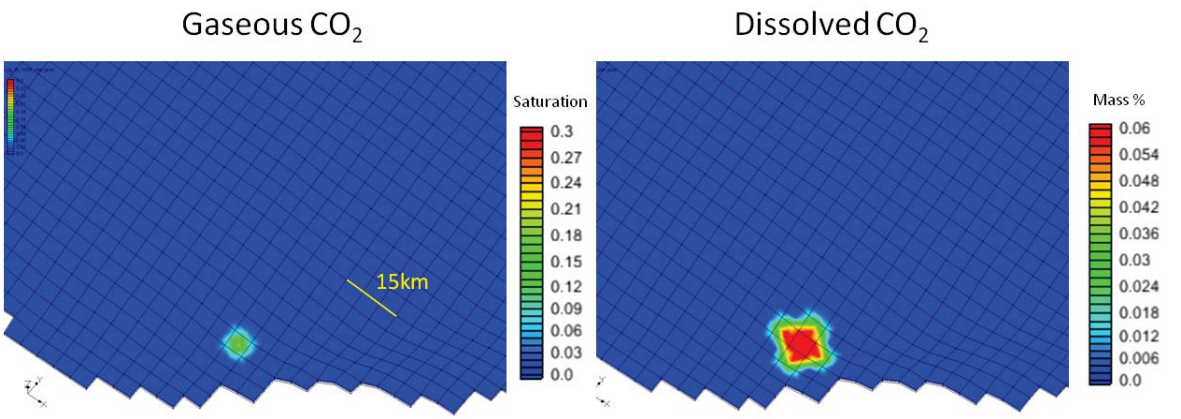

Figure 6. Case 1 - CO_2 plume and distribution of dissolved CO_2 (as mass fraction) at the end of year 1000.

The results show that the spreading of the CO_2 plume only takes place in a few grid blocks in the vicinity of the injection well. A pressure build-up (F_{op}) of 102% is observed at the injection grid at

the end of year 50. It should be pointed out that the grid is very coarse and the results can only be taken as indicative. The large grid size used for the injection region in this case will lead to an underestimation of the maximum overpressure at the injection location. In the subsequent cases, we have refined the grid to have cell sizes of 10-50 meters at the injection locations. This is deem adequate to yield reasonable estimates of maximum overpressure, given that the pressure drop across a radial distance of 50 is small compared to the overpressure at the injection location (This is due to the development of dry out zone with fully saturated low viscosity CO_2).

18.3.2 Case 2 and Case 3

Studies of the cap-rock characteristics, presented elsewhere in this report indicate best cap-rock integrity in the southern part of the domain. Therefore this domain was selected for the subsequent modeling studies. A finer grid was created using gradual grid refinement at the vicinity of the injection well. The first cases for this domain, Cases 2 and 3, only considered one variable thickness layer in the vertical direction. The difference between the cases was the character of the lower boundary that was closed in Case 2 and open in Case 3.

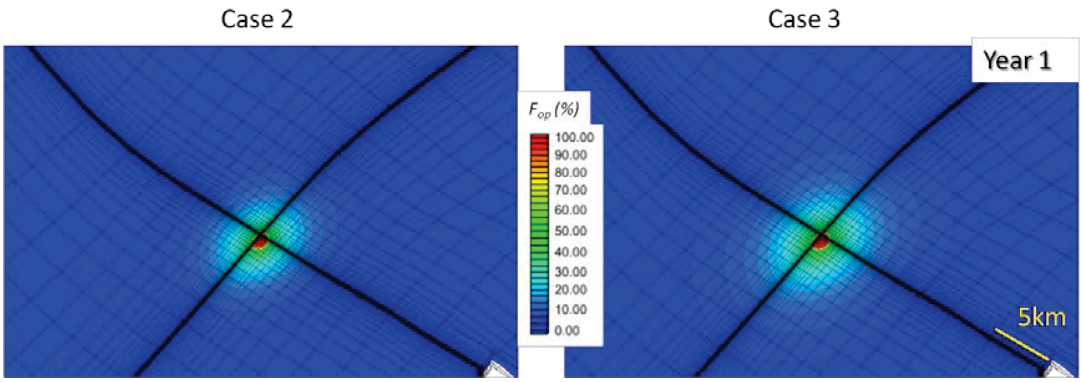

Figure 7. Cases 2 and 3 - Pressure build-up, presented as the overpressure in relation to the original in-situ pressure, after 1 year CO_2 injection.

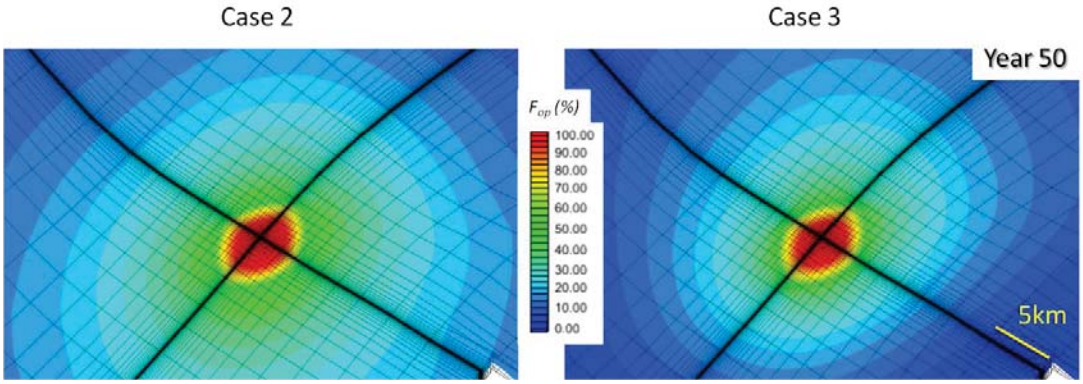

Figure 8. Cases 2 and 3 - Pressure build-up, presented as the overpressure in relation to the original in-situ pressure, after 50 year CO_2 injection.

Simulated pressure evolution, presented as overpressures in relation to the original in-situ pressure are shown in Figures 7 and 8. The pressure plumes from both cases are identical at the beginning of the injection (at year 1). Over pressure factors, F_{op} of 150% and 148% are observed at the injection blocks for Case 2 and Case 3, respectively.

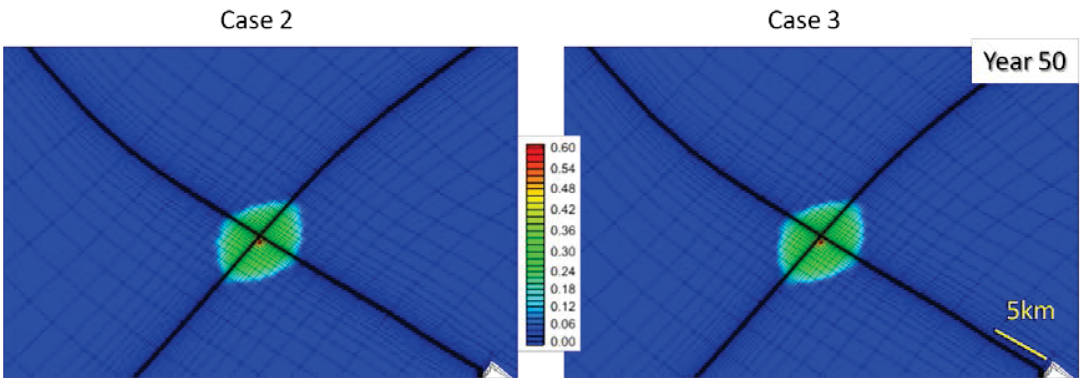

Figure 9. CO_2 saturation at the end of injection (year 50).

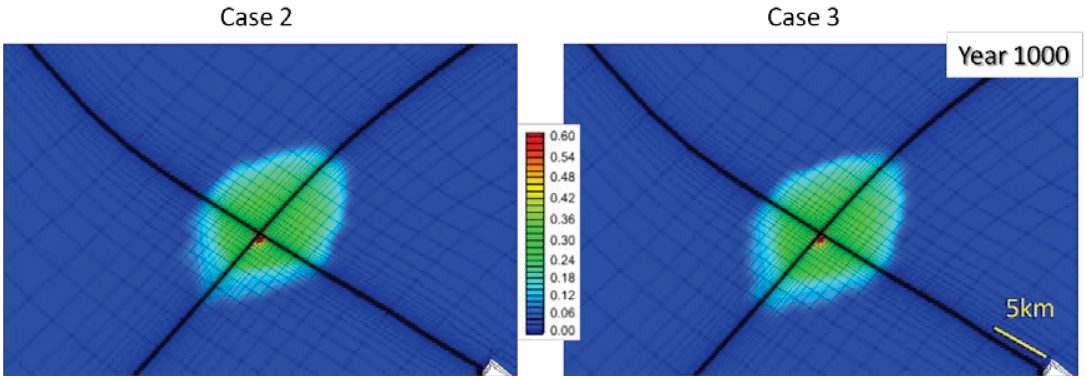

Figure 10. CO_2 saturation at the end of simulation (year 1000).

Identical CO_2 plumes are observed for Case 2 and Case 3 at the end of injection. At the end of simulation (year 1000) the up-dip CO_2 migration is observed for both cases but the trend is more obvious in Case 2. This is caused by the close boundary (A-C). Overall, the differences in these simulations due to the different lower boundary conditions are very small.

18.3.3 Case 4

Due to the significant pressure build-up observed in previous simulation runs, the injection rate was halved to 0.5 Mt CO_2 per year (at Inj_2) in the further simulations. A closed boundary condition at A-C (as in Case 2) was identified as a more conservative assumption, and thus again considered in Case 4.

In order to better resolve the migration pattern of the injected CO_2, a vertical discretization was also implemented. The modeling domain was divided equally in the vertical direction into seven layers. The injection well was perforated in the bottom-most section where the CO_2 injection is assumed to take place.

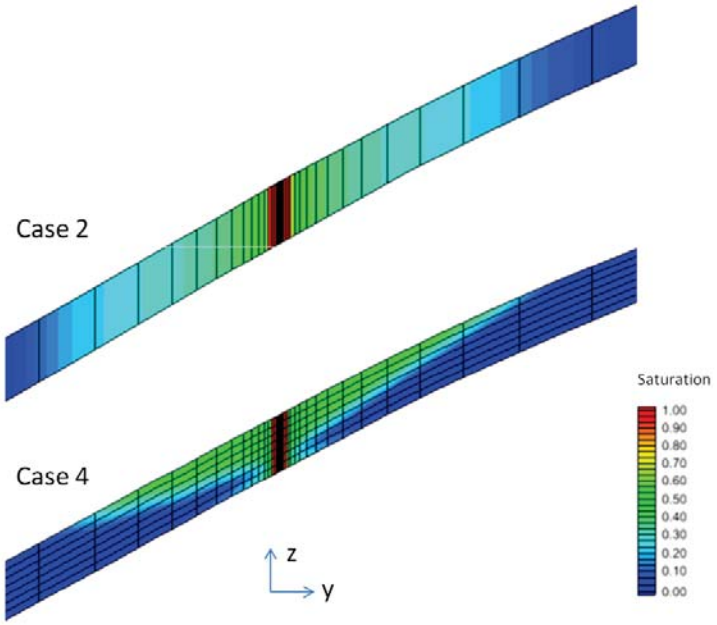

Figure 11. Case 4 - CO_2 saturation at the end of injection (Year 50). The figures show east-west view at the cross section of the injection block. (Exaggeration in z by 25)

It can be observed that the injected gaseous CO_2 migrates into the upper part of the aquifer as the gaseous phase CO_2 is lighter than the formation brine. As CO_2 migrates preferably in the uppermost layer, less formation volume is used by the CO_2 and this leads to a larger plume size compared to Case 2. The size of CO_2 plume in Case 4 is similar to that observed in Case 2 even though the injection rate is halved in Case 4 in comparison to Case 2. Some CO_2 spreading in the bottommost section is also observed in Case 4. This phenomenon is likely related to the still relatively coarse discretization. Further studies could address this, but the results shown in Figure 11 are nevertheless deemed to give a good estimation of overall plume spreading.

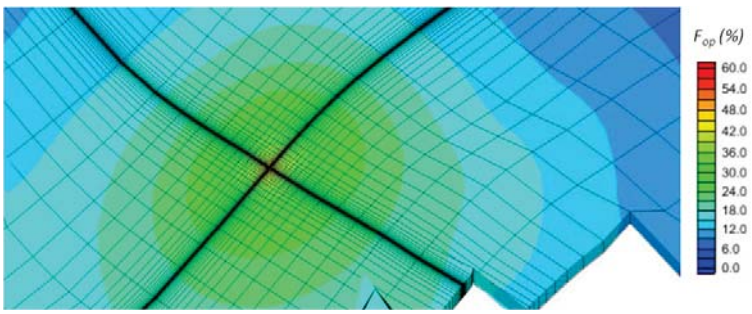

Figure 12. Case 4 - Pressure profile at the end of injection (top section, Year 50).

Maximum observed pressure build-up observed in the vicinity of the well was 59% (Figure 12). It should be pointed out that even though the injection location is in the bottom section of the well, the pressure profile does not vary significantly in the vertical direction.

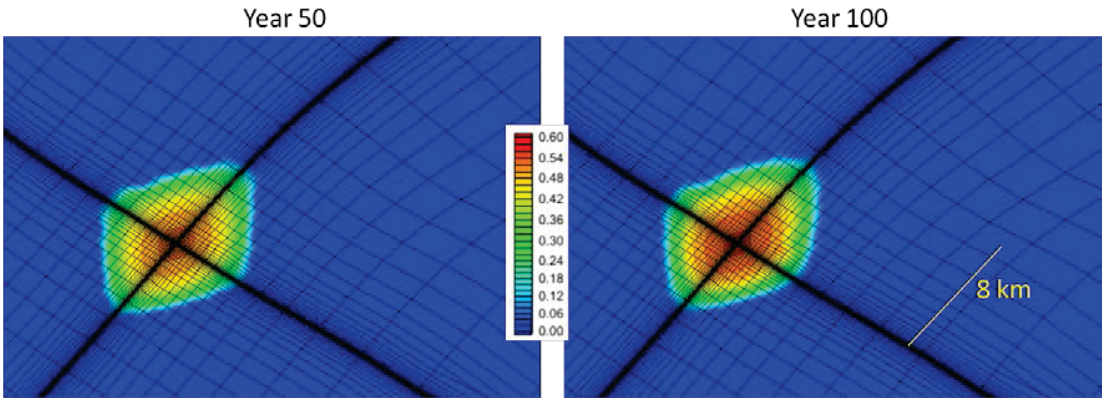

Figure 13. Case 4 - CO_2 saturation at the end of 50-year injection (left panel) and at the end of year 200 (right panel). Note that only the top section is shown in these figures.

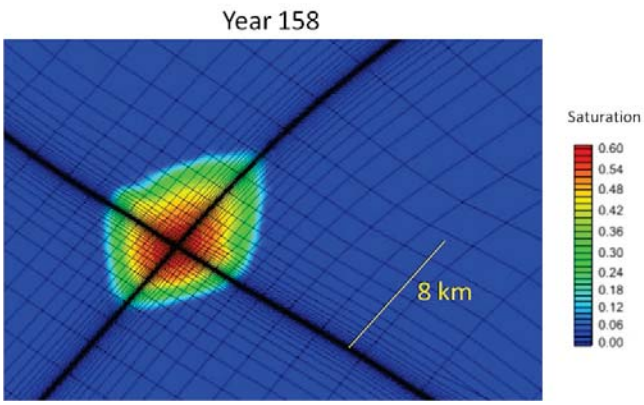

Figure 14. Case 4 - CO_2 saturation at end of year 158.

Figures 13 and 14 show the CO_2 plume spreading at the end of injection (50 years) and at 100 and 158 years. These TOUGH2MP runs were stopped at year 158 due to the time limits of the computation. The results show that during the last 100 year period the plume front has moved less than the length of one grid block in the up-dip direction. The plume front at the end of simulation is less than 8 km up-dip from the injection well. The dilution of the plume can also be observed, caused by the residual trapping and dissolution into formation water.

18.3.4 Case 5

Three injection wells were considered in this last scenario. The model used in Case 4 was modified by adapting grid refinements in the vicinity of all three injection wells. The initial and boundary conditions were the same as the ones used in Case 2. The following are preliminary results from the TOUGH2MP simulation runs, showing the pressure and CO_2 saturation evolution at the end of the 50 years injection. Due to the extensive character of these simulations, the evolution after the end of the injection are not included into the present report but will be presented in subsequent works.

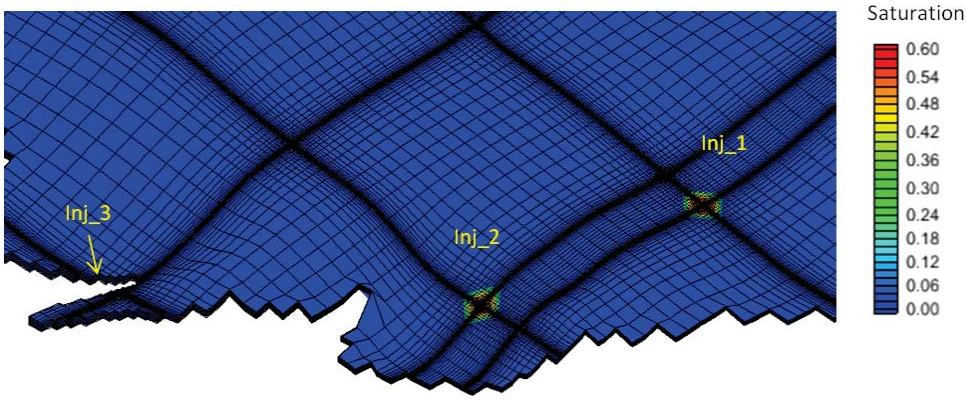

Figure 15. Case 5 - CO_2 saturation at the end of 50-year injection (top section).

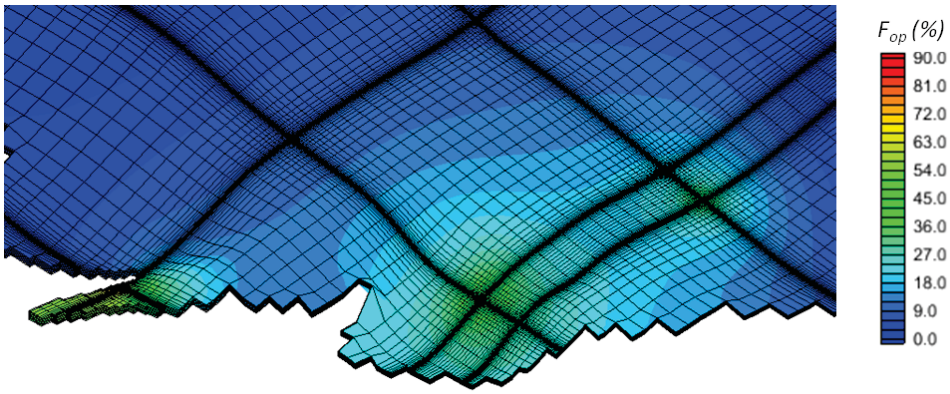

Figure 16. Case 5 - Pressure profile at the end of 50-year injection (top section).

The plume shape at the central injection well (inj_2) is similar to the one observed in Case 4. A pressure buildup of about 60% is observed at inj_2. This is in line with the analytical solution from Part A .When comparing with the results of Case 4, it can be seen that the influence from nearby injection well to the maximum pressure is quite small, which is due to the relative large distance (about 47 km) to the nearest injection well, inj_1. The maximum pressure increase is about 88%

(averaged in the vertical direction) at inj_3 where the lowest permeability is identified among the three injection wells.

18.4 Concluding remarks

The strengths of the TOUGH2/ECO2N model include well-developed equations of state (EOS) for the CO_2-brine system, the ability to account for both dissolution of CO_2 into brine and evaporation of brine into the CO_2-rich phase as well as capability to handle complex geometries in a flexible manner. In the previous chapters the complexity of the modeling is gradually increased starting from coarse 2D and pseudo-3D simulations and proceeding to full 3D models. In terms of detailed CO_2 migration pattern, one has to rely on a full 3D model (TOUGH2MP), while the earlier versions allow preliminary estimates concerning the effects of boundary conditions etc. It should be mentioned that due to the still relatively coarse discretization the numerical dispersion effect will likely cause overestimation of CO_2 dissolution. Further studies should involve even more extensive grid refinement/grid convergence studies, which were beyond the scope and time limitations of the present study.

A very conservative residual gas residual saturation (S_{gr}= 0.05) was used in all the previous simulations. It is likely that the residual gas saturation will be larger, thus further reducing the plume spreading. All models were built assuming smooth caprock topography and impermeable cap-rock. Including a low-permeability cap-rock in the models would likely reduce the pressure increase while still not causing any undesired CO_2 transport to upper layers. Finally, isothermal conditions are assumed in all simulations. Thermal conditions do influence some of the relevant processes such as CO_2 dissolution into the formation brine, and non-isothermal conditions could be considered in future work when more data are available.

18.5 References

Borgia A, Cattaneo L, Marconi D, Delcroix C, Rossi EL, Clemente G, Amoroso CG, Lo Re F, & Tozzato E (2011) Using a MODFLOW grid, generated with GMS, to solve a transport problem with TOUGH2 in complex geological environments: The intertidal deposits of the Venetian Lagoon. *Comput. Geosci*. **37**, 783-790.

Doughty, C. (2007), Modeling geologic storage of carbon dioxide: Comparison of non-hysteretic and hysteretic characteristic curves, *Energy Convers. Manag.*, *48*(6), 1768–1781.

Leverett MC (1941) Capillary behaviour in porous solids. *AIME Trans*. **142**, 152-169.

Mathias SA, González Martínez de Miguel GJ, Thatcher KE, & Zimmerman RW (2011) Pressure buildup during CO_2 injection into a closed brine aquifer. *Transport in Porous Media* **89**, 383–97.

Mualem Y (1976) New Model for Predicting Hydraulic Conductivity of Unsaturated Porous-Media. *Water Resour. Res.* **12**, 513-522.

Pruess K, Oldenburg C, & Moridis G (1999) *TOUGH2 User's Guide, Version 2.0.* Report LBNL-43134, Lawrence Berkeley National Laboratory, Berkeley, California.

Pruess K & Spycher N (2007) ECO2N - A fluid property module for the TOUGH2 code for studies of CO_2 storage in saline aquifers. *Energy Conversion and Management* **48**, 1761-1767.

van Genuchten MT (1980) A Closed-Form Equation for Predicting the Hydraulic Conductivity of Unsaturated Soils. *Soil Science Society of America Journal* **44**, 892-898.

Zhang K, Wu Y, & Pruess K (2008) *User's Guide for TOUGH2-MP A Massively Parallel Version of the TOUGH2 Code*, Report LBNL-315E, Lawrence Berkeley National Laboratory, Berkeley, California.

Zhou, Q., J. T. Birkholzer, E. Mehnert, Y.-F. Lin, and K. Zhang (2010), Modeling Basin- and Plume-Scale Processes of CO2 Storage for Full-Scale Deployment, *Ground Water*, *48*(4), 494–514.

PART C

19.0 SIMULATION OF CO2 SPREADING AND RELATED PROCESSES WITH TOUGH2 MODEL – DALDERS STRUCTURE

Liang Tian, Fritjof Fagerlund and Auli Niemi

19.1 Model description

19.1.1 Description of the Dalders Structure

As for the Dalders Monocline, for Dalders Structure the static geological model and model parameter information for the simulations were provided by SLR. For the Dalders structure there was information available for vertical layering, for which reason the following layers (Table 1) were included into the simulation model.

Table 1. Sub-layer description

Layer	Thickness (m)	Lithology
Mid_Camb_1	56	Sandstone with shale influence
Mid_Camb_2	10	Sandstone
Mid_Camb_3	7	Sandstone with silt/shale
Mid_Camb_4	9	Sandstone
Mid_Camb_5	18	Sandstone with high shale content

Table 2. Summary of the averaged geohydrological properties for the layers

	layer 1	layer 2	layer 3	layer 4	layer 5
Porosity (%)	7,8	12,3	11,7	13,2	5,9
permeability (mD)	19,8	3	24,4	30,9	16,8
layer top (m)	-1425	-1470	-1480	-1487	-1496

19.1.2 Conceptual Model

A 3D model was built based on the 250m x 250 grid of the static model. For the numerical grid, the Mid_Camb_1 layer was further divided in the vertical direction into five sub-layers. Similar, the Mid_Camb_5 layer was divided into two sub-layers. The discretization resulted in a uniform grid of 250m × 250m grid blocks in the horizontal plane and a total of 10 sub-layers in the vertical direction (Figure 1). The total number of grid elements was 17490. The permeability, porosity, top elevation and bottom elevation were retained for each layer by linear interpolation from the static model provided by SLR

19.1.3 Initial and boundary conditions and simulation scenarios

The model domain is initialized by calculating a gravity equilibrium ambient condition. Salinity is assumed constant at 11.54% (wt. NaCl) in the whole domain. Isothermal condition is considered with a constant temperature of 50℃.

Impermeable top and bottom (closed boundary) condition are used as the boundary conditions for the top and bottom of modeling domain. For the lateral boundaries, the northern boundary (B-A-B') is identified coincides with fault lines and considered closed. The southern boundary (B-A'-B') is identified as spill point where the formation continues outside the modeling domain thus set open across all the sub-layers.

The injection of CO_2 is through one vertical well located in the middle, as shown in Figure 1. The well is assumed to be perforated in the bottommost section, where the injection takes place. Supercritical CO_2 is injected continuously for 20 years. The total simulation period is 1000 years. 0.3 $MtCO_2$ / year and 0.5 $MtCO_2$ / year are the two injection rates simulated, based on the semi-analytical calculations in Part A.

19.2 Numerical simulations

TOUGH2/ECO2N model is used to simulate the CO_2 injection and migration in the modeling domain (Pruess et.al, 1999; Pruess, 2005). A description of the modeling tool is given in Part B in connection to the simulations for the Dalders Monocline. The same Leverett scaling of capillary entry pressure is used here also. (Leverett, 1941)

19.3 Results and discussion

Figures 2 to 4 show the simulated pressure increase, CO_2 saturation and mass fraction of dissolved CO_2 at various times for the two injection rates.

Pressure build-up induced by the CO_2 injection is displayed using the overpressure factor (for definition, see Part B). Both 0.3 Mt and 0.5Mt scenarios show moderate pressure increase of less than 50% compared to the in-situ hydro-equilibrium pressure. The pressure increase is more prominent in the 0.5 Mt/year injection case and in both cases the pressure increase reaches the closed northern boundary, even though at low level.

The CO_2 plume front in Case 2 reaches the southern boundary at the end of Year 20. For Case 1 (0.3Mt / year), CO_2 plume front reaches the southern boundary at the end of Year 50. At the end of the 1000 years, the plumes from both cases have moved up-dip while remaining within the 11 km x 4 km observation window.

In Case 1 approximately 0.00005 % of the total CO_2 injected had escaped the model domain through the southern boundary by the end of year 50. In Case 2 the corresponding number is 0.11% of the total injected CO_2. At the end of the 1000 year simulation, the total migration over the formation boundary accounts for 0.15% in Case 1 and 1.96% in Case 2. This is an indication that the proposed injection location should be relocated or less CO_2 should be injected at this location. Further simulations are needed to assess the optimal location for injection wells in the Dalders structure. With an open boundary over which CO_2 migration should be avoided, the effective storage capacity here is limited by the amount that can be stored without migration over the boundary.

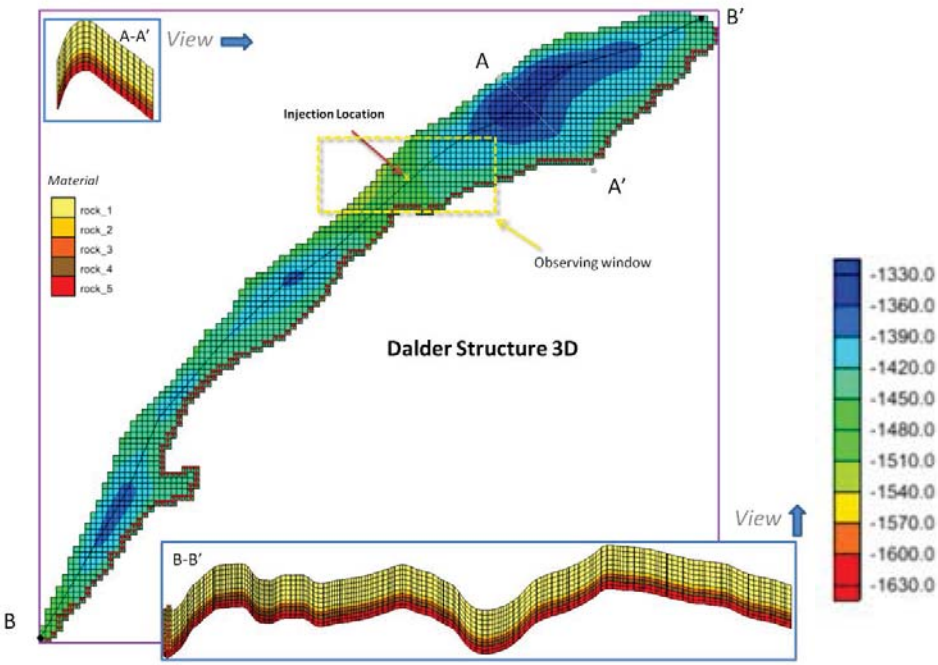

Figure 1. Dalders Structure - Conceptual model, grid and location of the injection well. Colors indicate the depth as expressed in meters in mean sea level.

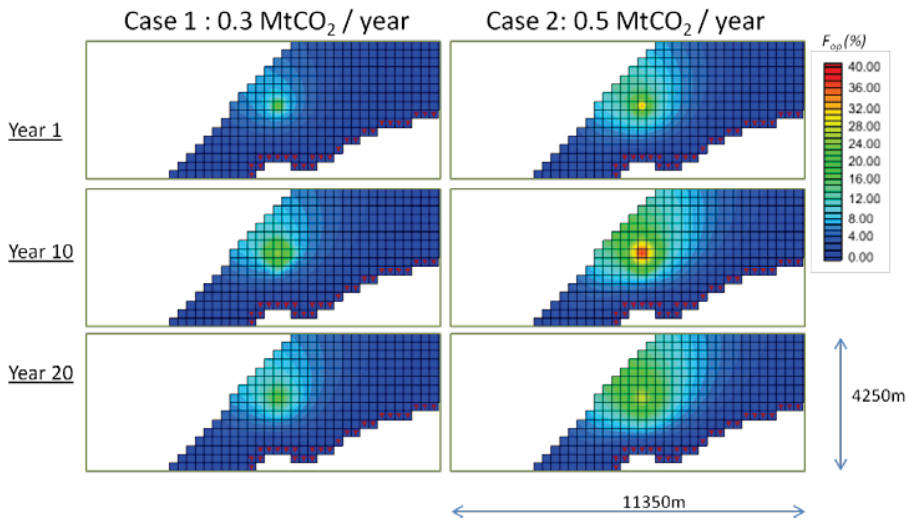

Figure 2. Pressure build-up (bottommost layer). The definition to F_{op} is given in section for Dalders Monocline model.

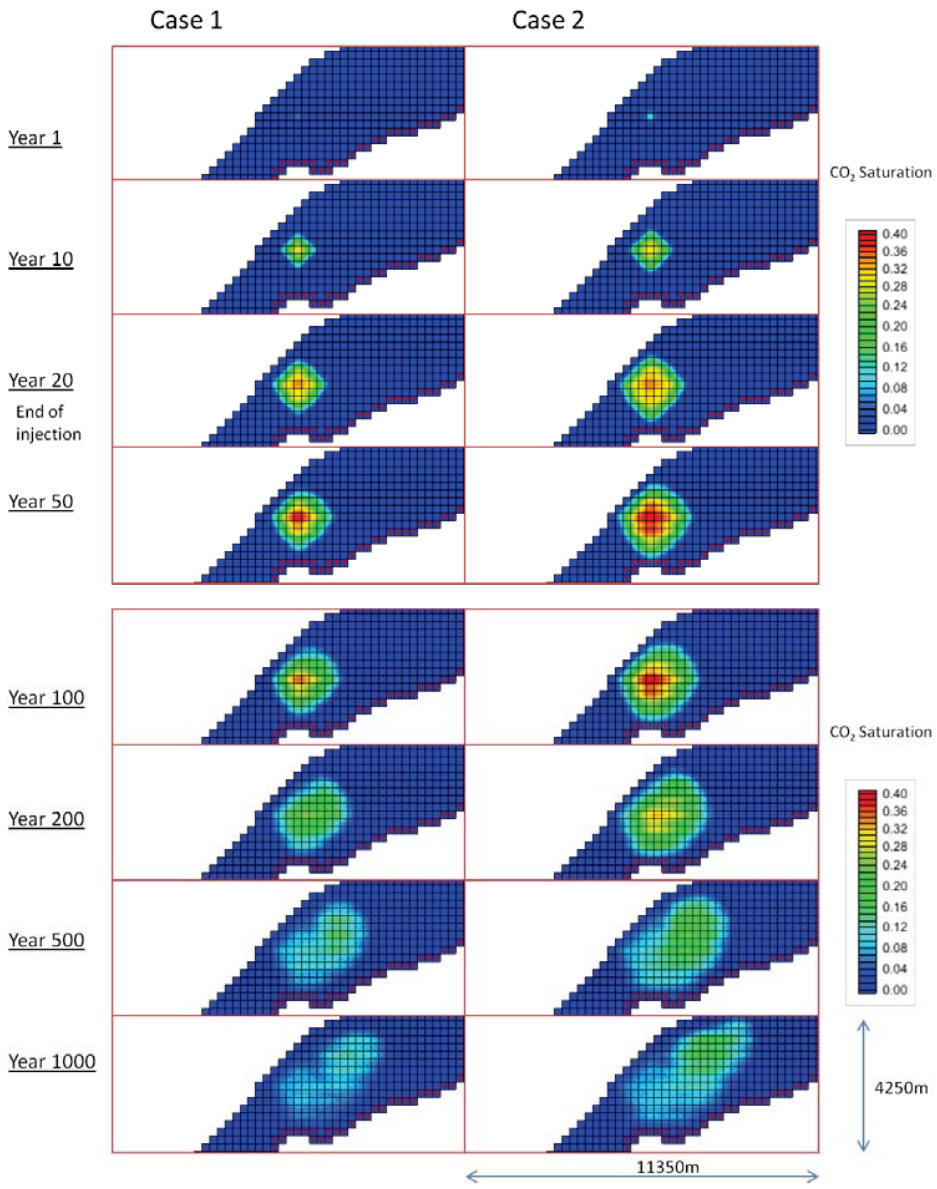

Figure 3. Saturation profile (top layer) at various times. Purple dots show the southern open boundary.

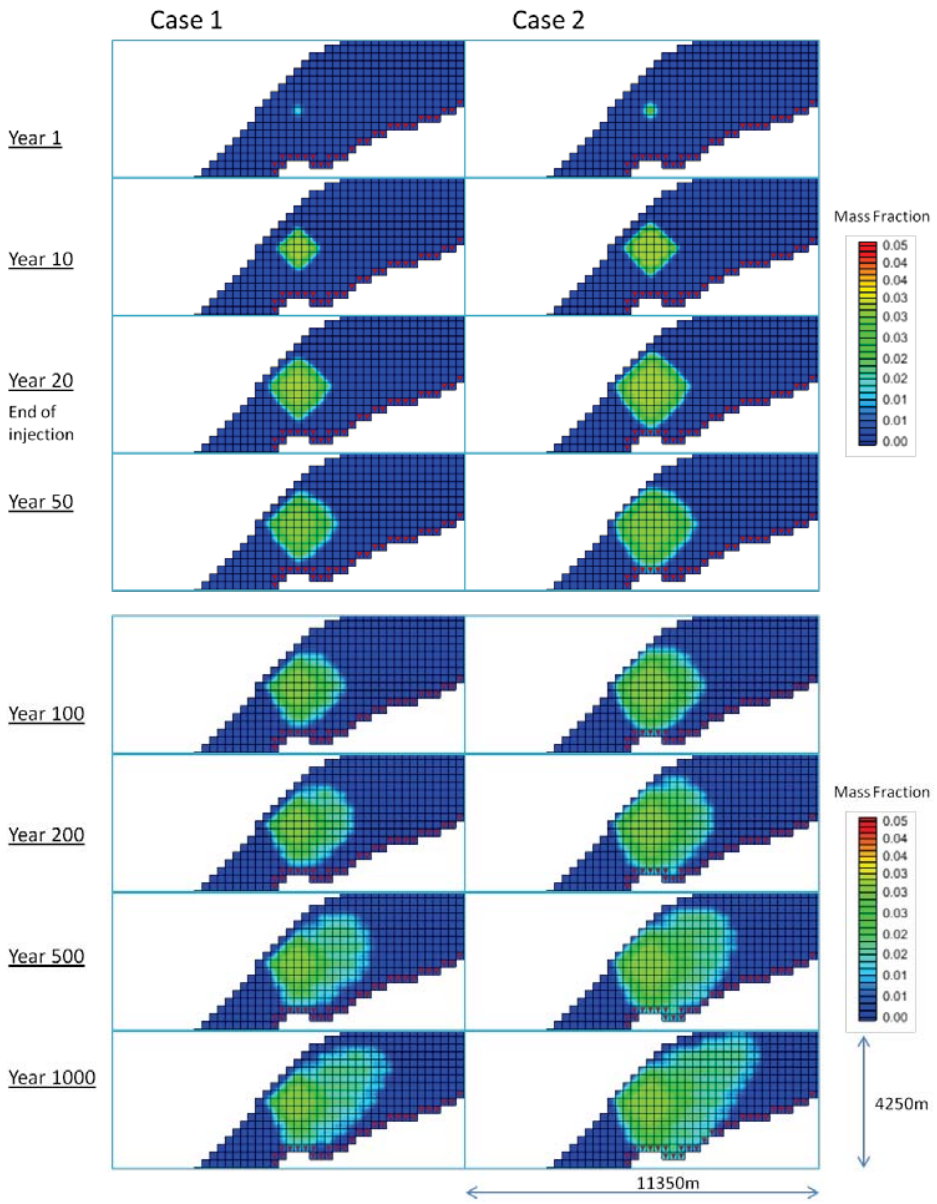

Figure 4. CO_2 dissolution (top layer) at various times. Purple dots show the southern open boundary.

19.4 References

Leverett MC (1941) Capillary behaviour in porous solids. *AIME Trans*. **142**, 152-169.

Pruess K, Oldenburg C, & Moridis G (1999) *TOUGH2 User's Guide, Version 2.0.* Report LBNL-43134, Lawrence Berkeley National Laboratory, Berkeley, California.

Pruess K & Spycher N (2007) ECO2N-A fluid property module for the TOUGH2 code for studies of CO_2 storage in saline aquifers. *Energy Conversion and Management* **48**, 1761-1767.

PART D

20.0 TOPOGRAPHIC EFFECTS OF CO_2 PLUME MIGRATION AND INJECTION PRESSURE ESTIMATION: APPLICATION OF VERTICAL EQUILIBRIUM MODEL TO DALDERS MONOCLINE AND DALDERS STRUCTURE IN BALTIC SEA

Byeongju Jung and Auli Niemi

20.1 Introduction

In this Chapter we present results from so-called vertical equilibrium model as applied to investigate CO_2 spearing and related pressure increase in the Dalders monocline and Dalders structure in Baltic Sea. For this we developed a computational model based on our earlier numerical modes. Our model assumes vertical equilibrium of pressure (Bear, 1972) and enables to consider variable density and viscosity depending on pressure and temperature. The vertical equilibrium approach was originally developed to predict regional groundwater movements in unconfined aquifers, but later extensively used by oil industry due to its accuracy and computational simplicity (Gray *et al.* 2012). Recently, this method is spotlighted again and used for CO_2 injection projects based on the similarity of physical properties of supercritical CO_2 phase and liquid petroleum in a certain condition (Gasda *et al.* 2009; Szulczewski & Juanes 2009; Juanes *et al.* 2010; Gasda *et al.* 2012a; 2012b). The approach implemented in our numerical model follows these CO_2 application approaches.

20.2 Vertical Equilibrium Model for CO_2 Migration

One of the merits using vertical equilibrium approach is the computational efficiency compared to a full 3D model, such as the TOUGH2 simulations presented in Parts B and C of this report. The VE model can, however, include enough complexity to produce more accurate solutions than the available analytical approaches, including the topographic information of the caprock and variable fluid density and viscosity depending on P-T conditions. These factors are important for predicting the fate of the injected CO_2 due to the importance of the buoyancy forces for CO_2 migration.

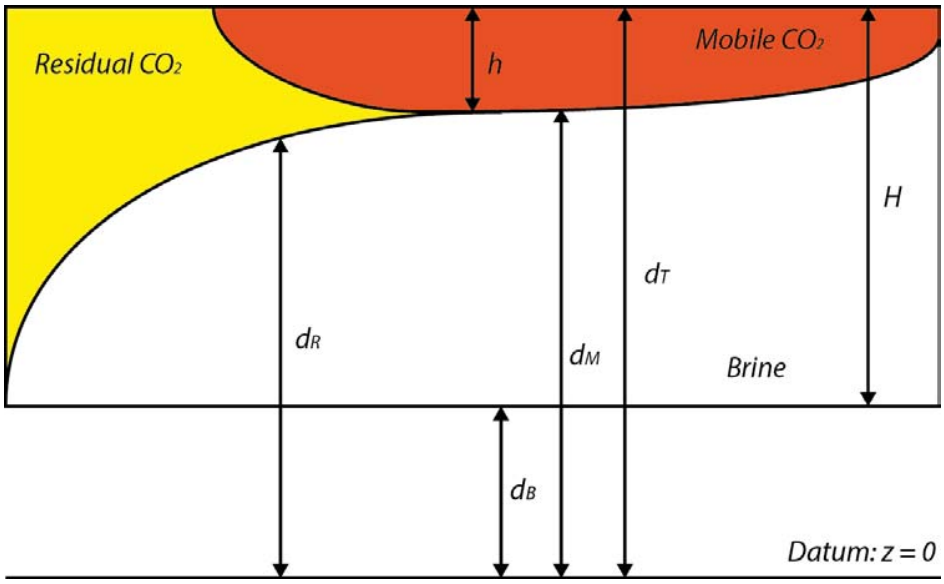

Figure 1. Schematic diagram showing the vertical structure of migrating CO_2 plume after injection (modified from Gasda et al., 2009). *H* is the confined aquifer thickness, d_T is the distance between the datum to the top of the aquifer, d_B is the distance to the bottom, d_M and d_R represent the distances from the datum to mobile and residual CO_2 plume.

To use the VE approach for dynamic modeling of CO_2 spreading, hydrogeological parameters including permeability, porosity, and compressibility need to be averaged over aquifer thickness. Also, the target aquifer needs to be assumed vertically homogeneous and confined. The capillary pressure between phases and the dissolution of CO_2 were not considered in this study.

To derive the governing equations, we start with the 3D system with two separate phases, which are the non-wetting (CO_2-rich) phase (*c*) and the wetting (brine) phase (*b*), having a sharp interface in the confined aquifer of thickness *H*. The distances between the datum to the top of the aquifer is d_T, and to the bottom is d_B. d_M and d_R represent the distances between the datum and the mobile and residual CO_2 plumes, respectively. Thus, the depth of mobile CO_2 plume, $h = d_T - d_M$ (Fig. 1).

Beginning with the conservation of mass for each phase (α) in the system, where $\alpha = b, c$, we can write (Bear, 1972)

$$\frac{\partial(\phi\rho_\alpha S_\alpha)}{\partial t} = \nabla \cdot (\rho_\alpha \mathbf{q_\alpha}) = \rho_\alpha F_\alpha \qquad (1)$$

where ϕ is the porosity, S_α is the saturation, ρ_α is the density of fluid, F_α is the source and sink term (volume per time), and $\mathbf{q_\alpha}$ is the volumetric flux.

After the standard vertical averaging procedure, we can write (Gasda *et al.* 2009),

$$\phi\rho_b\bar{\beta}_b(H-h)\frac{\partial p_b}{\partial t}+\phi\rho_b(1-S_{res}^b)\frac{\partial(H-h)}{\partial h} \tag{2}$$

$$+\nabla\cdot\rho_b\bar{\mathbf{q}}_\mathbf{b}-\rho_b q_b|_{d_T}-\rho_b q_b|_{d_B}=\int_{d_B}^{d_M}\rho_b F_b dz$$

$$\phi\rho_c\bar{\beta}_c h(1-S_{res}^b)\frac{\partial p_c}{\partial t}+\phi\rho_c(1-S_{res}^b)\frac{\partial h}{\partial t} \tag{3}$$

$$+\nabla\cdot\rho_c\bar{\mathbf{q}}_\mathbf{c}+\rho_c q_c|_{d_T}-\rho_c q_c|_{d_B}=\int_{d_M}^{d_T}\rho_c F_n dz$$

In above equations, $\bar{\beta}_\alpha$ is the vertically-averaged bulk compressibility of phase α and porous media, and S_{res}^b is the residual wetting phase saturation. The vertically-averaged volumetric flux, $\bar{\mathbf{q}}_\boldsymbol{\alpha}$ can be calculated using Darcy's law as below

$$\bar{\mathbf{q}}_\boldsymbol{\alpha}=-\frac{H\bar{\mathbf{k}}_{\mathbf{r}\boldsymbol{\alpha}}\,\mathbf{k}}{\mu_\boldsymbol{\alpha}}\nabla p_\alpha \tag{4}$$

where $\bar{\mathbf{k}}_{\mathrm{r}\alpha}$ is the pseudo relative permeability obtained from the phase average over the thickness of phase α, and $\mathbf{k}$ is the vertically averaged intrinsic permeability.

20.3 Model - Dalders Monocline

20.3.1 Model Settings

The target area modeled for the CO_2 injection is the deep part of the Dalders monocline (Fig. 2). The modeled units are the lower and middle Cambrian units, which have relatively high permeability and porosity, and are mostly continuous within the monocline area. From above the aquifer is sealed by thick Ordovician units and Alum shale that can work as excellent caprocks for the injected CO_2 plume. The thickness of Cambrian units varies depending on locations, but generally the structure becomes thinner and pinches out by moving northward. The overall thickness in the deepest part is about 100 m.

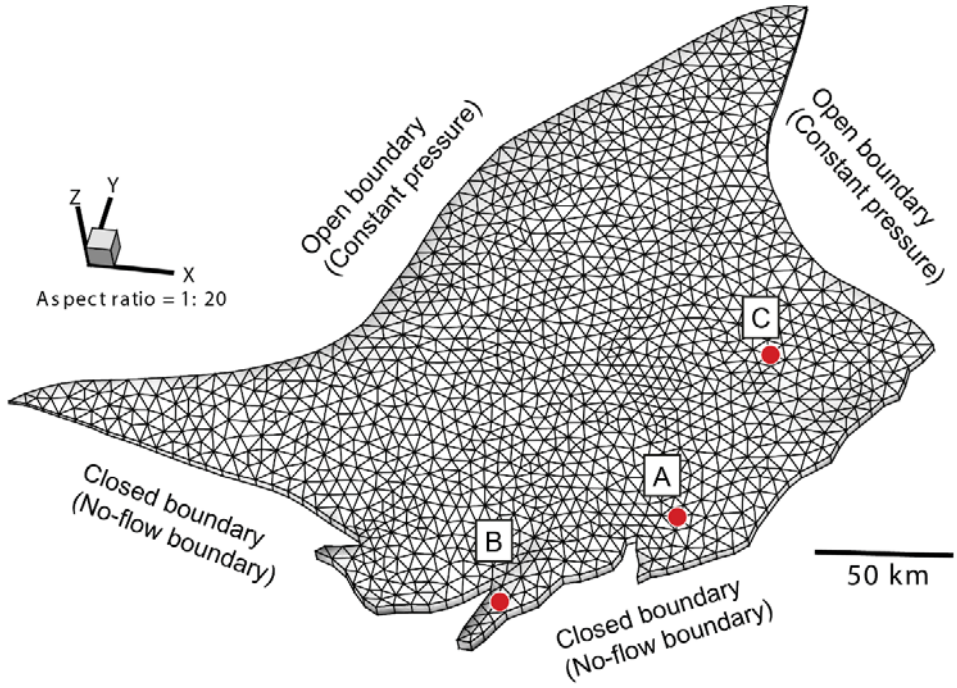

Figure 2. Numerical grid used in the simulation. The CO_2 injection wells are marked in red circles near the southern boundary.

The southern side of the monocline is bounded by a fault zone, and the sedimentary units in the northern side are exposed in the submarine/atmosphere. We assume the southern boundary of the modeling domain to be closed (no-flow boundary condition) and the northern boundary to be open (constant-pressure boundary condition). The hydrogeological parameters (e.g. permeability, porosity) used in the model were obtained from several boreholes spread over the monocline. The permeability ranges tens to one hundred millidarcy. An isothermal temperature ~ 50˚C was assumed for the whole area, and CO_2 density and viscosity were calculated using given pressure and temperature. Relative permeability functions used in the model is linear with respect to vertically averaged saturation (Gasda et al. 2009). Irreducible CO_2 saturation (Sgr) was set to 0.2.

Three different scenarios were tested to investigate the pore pressure development and the CO_2 plume migration during and after the injection: (1) *Scenario 1* – Single-well injection to well A with the rate of 0.5 Mt CO_2/year, (2) *Scenario 2* – Multiple-well injection to wells A, B, and C with the rate of 0.5 Mt CO_2/year, and (3) *Scenario 3* – Multiple-well injection to wells A, B, and C with the rate of 1.0 Mt CO_2/year. The injection periods for all scenarios are 50 years.

20.3.2 Pressure Distribution and CO_2 Plume Migration - Dalders Monocline

Single-well Injection (Scenario 1)

The overpressure ratio was used for plotting fluid pressure increase due to the CO_2 injection.

$$\lambda(\%) = \frac{P_F - P_H}{P_H} \times 100 \tag{5}$$

where λ is overpressure ratio in percentage, P_F is pore fluid pressure, and P_H is hydrostatic pressure.

During the CO_2 injection (0 ~ 50 years), pore fluid pressure around the injection well increases gradually (Fig. 3). The overpressure ratio reaches at the injection well A reaches a maximum value of 89%, after 50 years of injection. The overpressured area also increases with the injection time, and the diameter of 50% overpressured zone becomes about 20 km after 50 years. The shape of the influencing zone is roughly concentric circles bounded by the fault zone.

Overall CO_2 plume diameter is less than 10 km and shows no significant movements during relatively long recovery period after the end of injection (~ 500 years) (Fig.4). The thickness of mobile CO_2 is about 2.0~2.2 m around the injection well and gradually decreases with increasing distance from the center. A small migration of the plume toward the north is detected, but could be considered minor regarding the size of the monocline structure.

Multiple-well Injection (Scenarios 2 and 3)

In these scenarios we simultaneously injected CO_2 into three wells with the rate of 0.5 Mt/year for 50 years (Scenario 2), which are the same rate and period than in the previous single-well scenario (Scenario 1). During the injection, the overpressured areas first (at 20 years) appear as isolated patches, and then (at 50 years) becoming combined into a broader area of overpressure, with higher overpressure ratio in each of the injection wells (Fig. 5). The overpressure ratio in wells A and C is after 50 years ~90% and in the area between the wells is in the order of 20~30%. The injection well C shows a clearly higher overpressure ratio, due to its location close to the closed fault zone and low permeability. In the well C, the maximum overpressure ratio is 230% after 50 years of injection.

The CO_2 plumes created by the multiple-well injection are similar to that by the single-well (Fig. 6). The diameter of each plume is less than 10 km. The thickness of mobile CO_2 plume in the well C is deeper than other two wells because of the low permeability and porosity values of the targeted aquifer. Significant migration was not observed after a relatively long time period after the end of injection (~ 500 years).

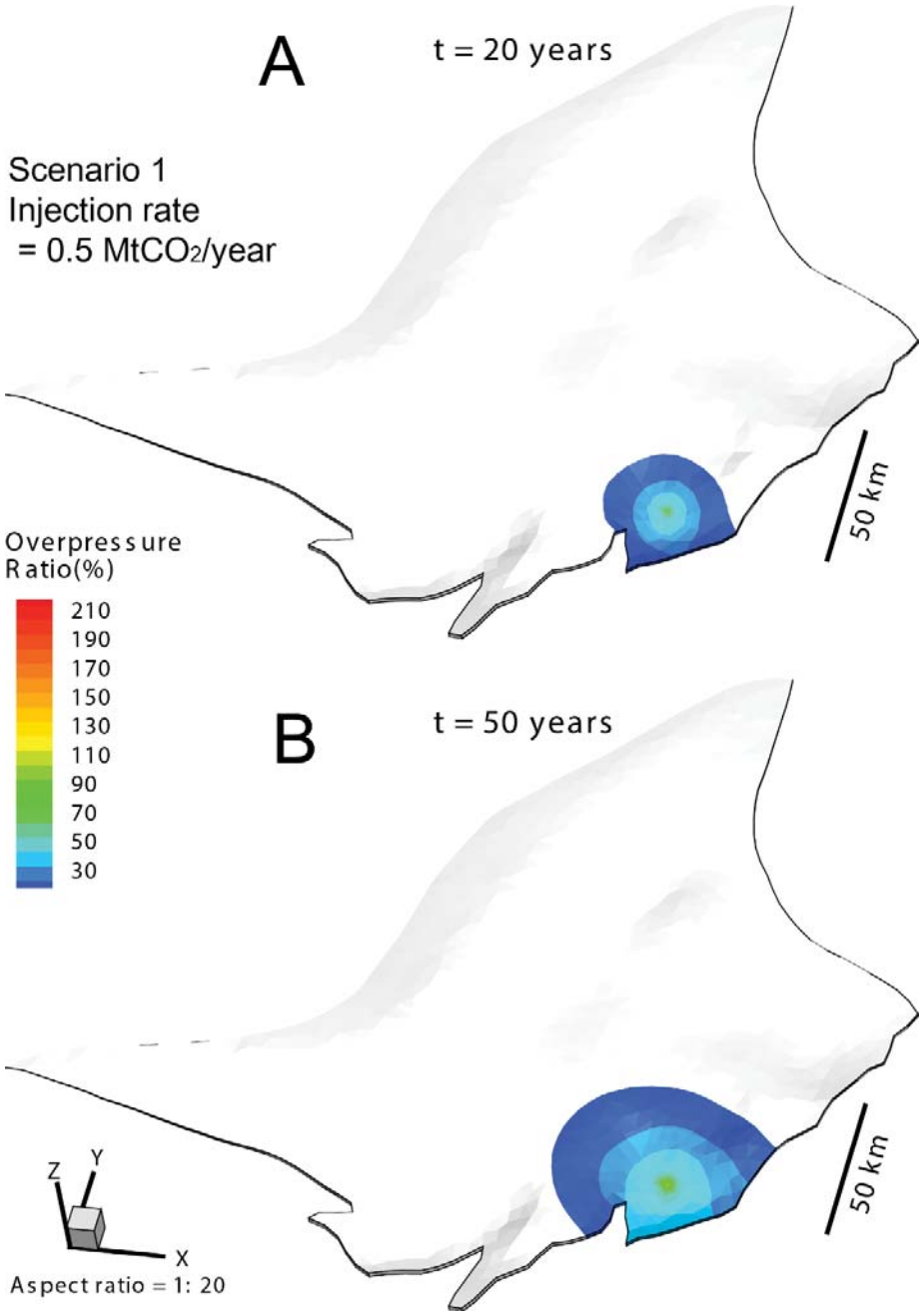

Figure 3. Scenario 1 - Overpressure ratio by the single-well CO_2 injection with the rate of 0.5 Mt CO_2/year for 50 years (Scenario 1). (a) 20 years after injection, (b) 50 years after injection.

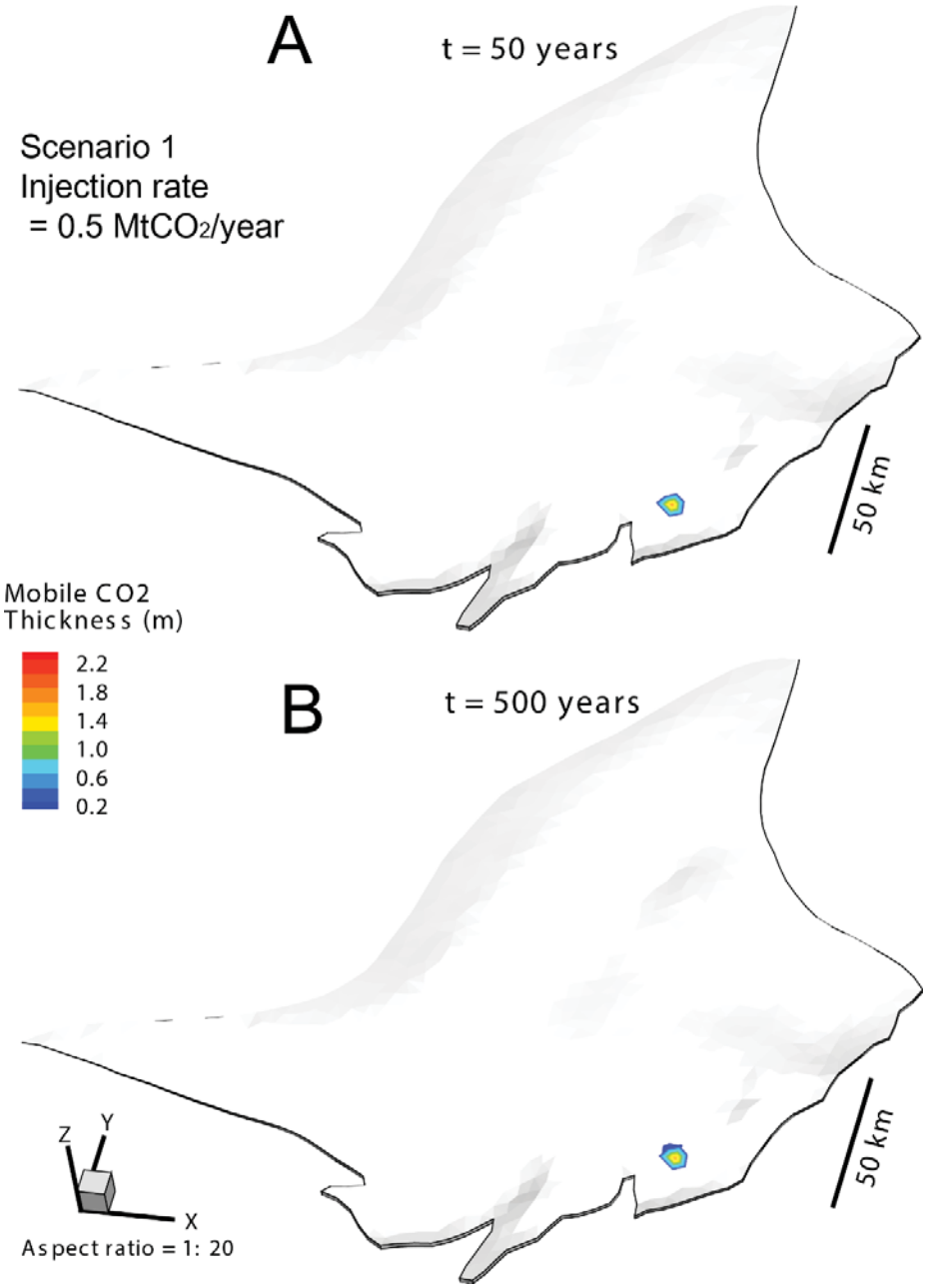

Figure 4. Scenario 1 - Mobile CO_2 plume migration by the single-well injection with the rate of 0.5 Mt CO_2/year for 50 years (Scenario 1). (a) 50 years after injection, (b) 500 years after injection.

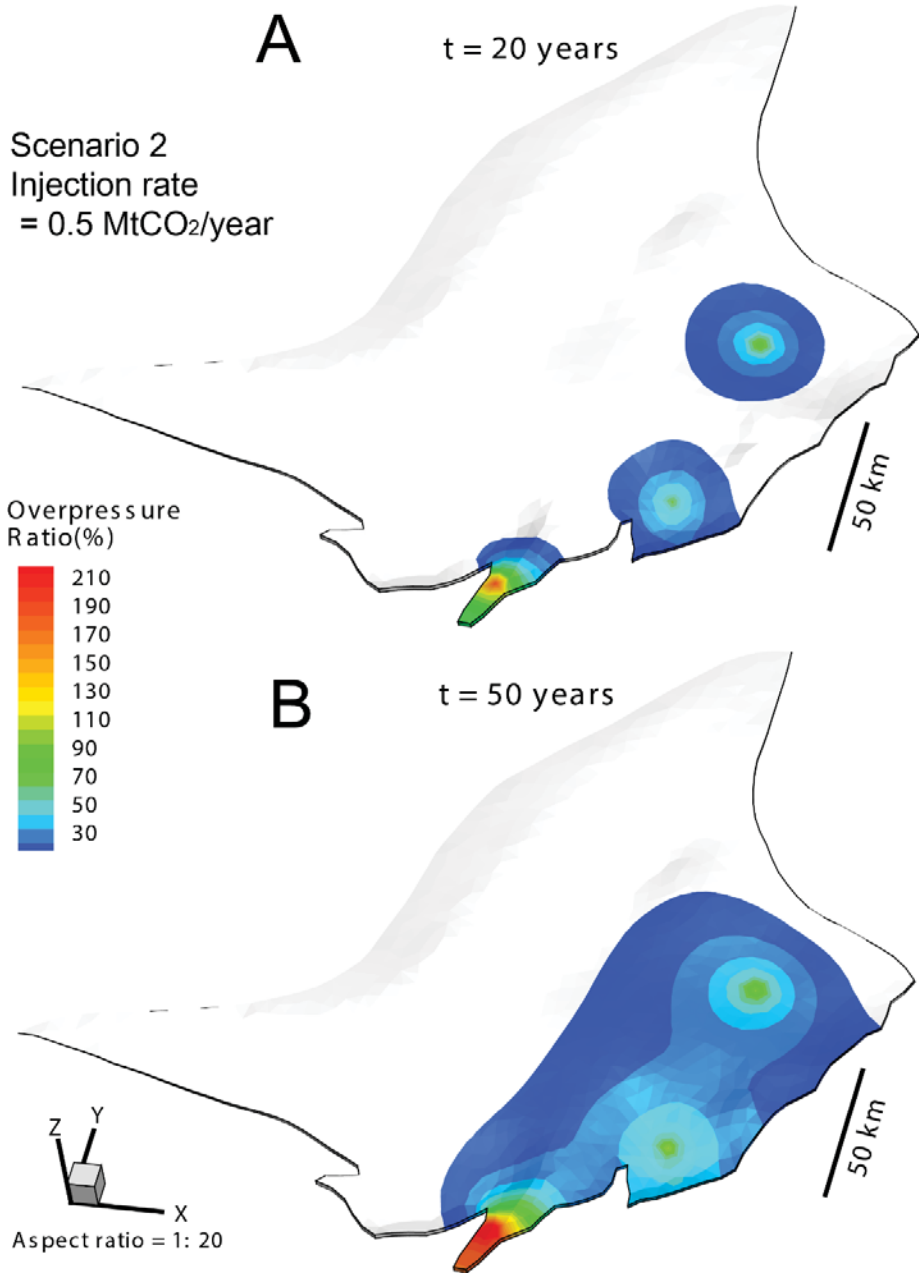

Figure 5. Scenario 2 - Overpressure ratio by the multiple-well CO2 injection with the rate of 0.5 Mt CO2/year per well for 50 years (Scenario 2). (a) 20 years after injection, (b) 50 years after injection.

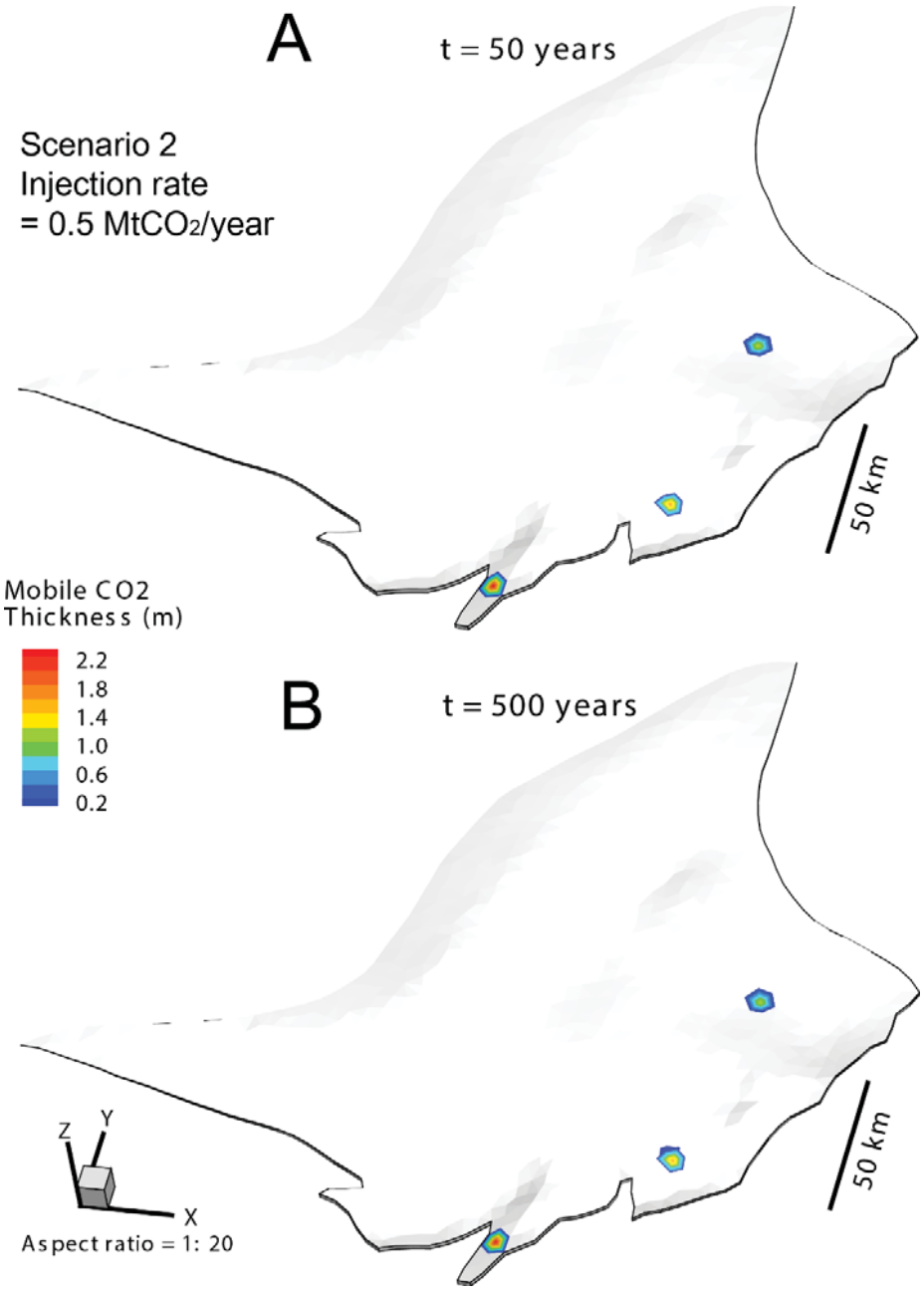

Figure 6. Scenario 2 - Mobile CO2 plume migration by the multiple-well CO2 injection with the rate of 0.5 Mt CO2/year per well for 50 years (Scenario 2). (a) 50 years after injection, (b) 500 years after injection.

In Scenario 3, the injection rate for all three wells is increased to 1.0 Mt/year. The overpressure ratio at the injection wells increased to ~180% (A and C) and the influence area was wider compared to the overpressure distribution from Scenario 2 (Fig. 7). Highly overpressured area around the well C was also expanded in case of the increased injection rate and the maximum value was over 300%.

Increasing the injection rate also influences the size of the CO_2 plume. The maximum thickness of the plume increased to about 4.0 m, and the diameter of the area also increased to about 15 km (Fig. 8). Much more prominent plume migration is observed compared to that from the Scenario 2, although it is still not significant considering the scale of the monocline structure. The overall direction of migration is from south to the north, due to topographic reliefs of the monocline.

20.4 Model - Dalders Structure

20.4.1 Model Settings

This area is an anticline structure attached to the southern part of the Dalders monocline, consisting of Cambrian sedimentary units (Fig. 9). Thick low-permeable Ordovician sequences and shale layers generally provide a good sealing capacity for the CO_2 storage. The average thickness of lower to middle Cambrian sandstone is about 1 km. The depth ranges 1.3 ~ 1.4 km below sea level, and the physiographic map shows three high locations suitable for commercial size CO_2 injection operation.

The northern boundary of the structure is a closed fault zone and considered a closed boundary (no-flow boundary condition). The southern boundary is a spill point, and assumed as an open boundary (constant pressure boundary condition). The location of the injection well (D) was chosen in the middle of the structure where the depth is relatively deep; hence we can easily observe the overpressure development and migration induced by the CO_2 injection. The injection rate and period applied to the well D are 0.3 Mt/year for 50 years.

20.4.2 Pressure Distribution and CO2 Plume Migration: Dalders Structure

The overpressure ratio at the injection well is about 20%, and the influencing area is extended along the northern boundary due to the sealing effect by the closed fault (Fig. 10). The pressure response is relatively fast during the injection due to relatively high permeability of this region (50~80 md).

The size of mobile CO_2 plume after 50 years is about 3~4 km with 7.0 ~ 10.0 m thickness, and the plume slowly moves towards the higher elevation due to the buoyancy (Fig. 11). After 500 years, the plume has migrated further to the north (topographically higher location) and elongated along the center line of the structure.

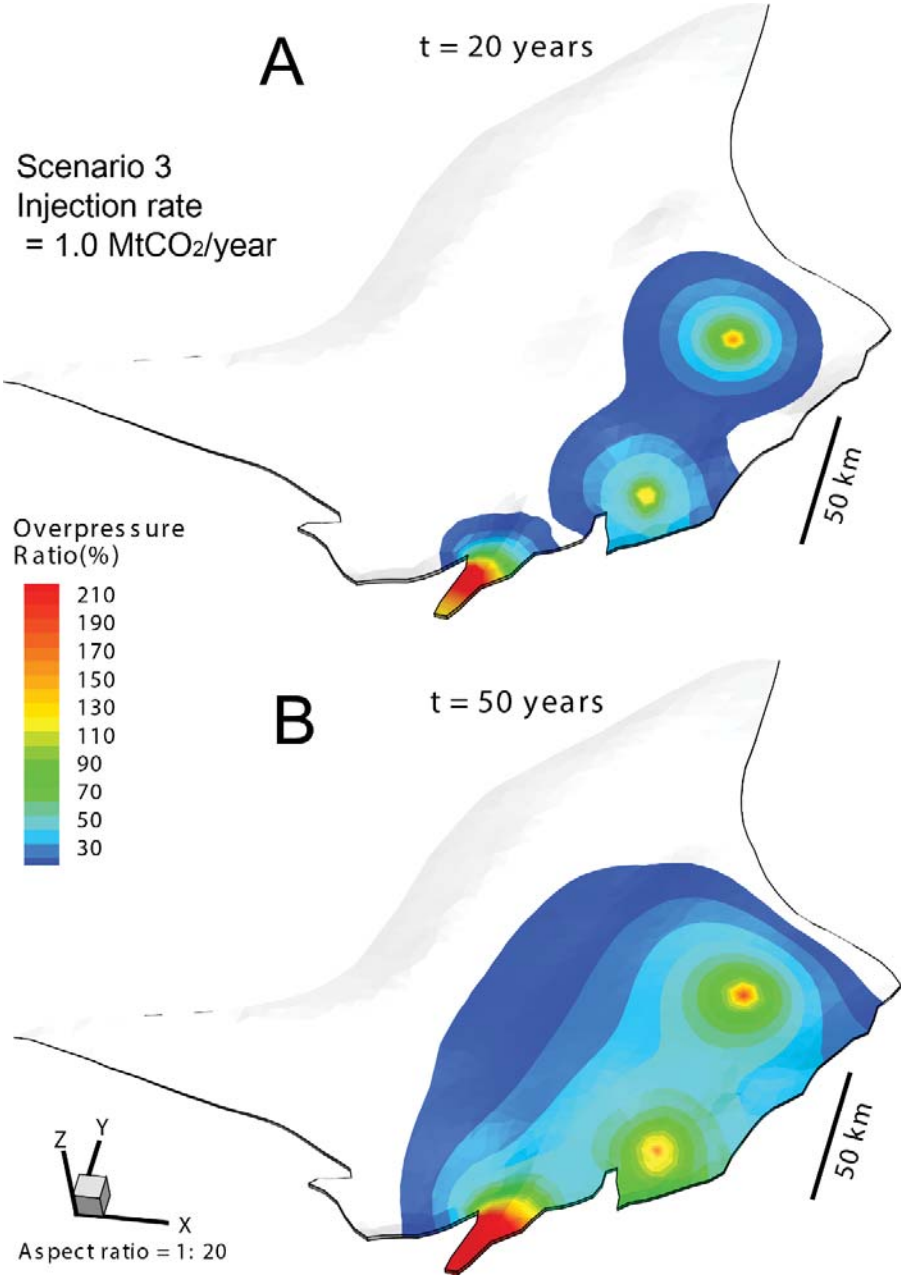

Figure 7. Scenario 3 - Overpressure ratio in the multiple-well CO_2 injection with the rate of 1.0 Mt CO_2/year per well for 50 years (Scenario 1). (a) 20 years after injection, (b) 50 years after injection.

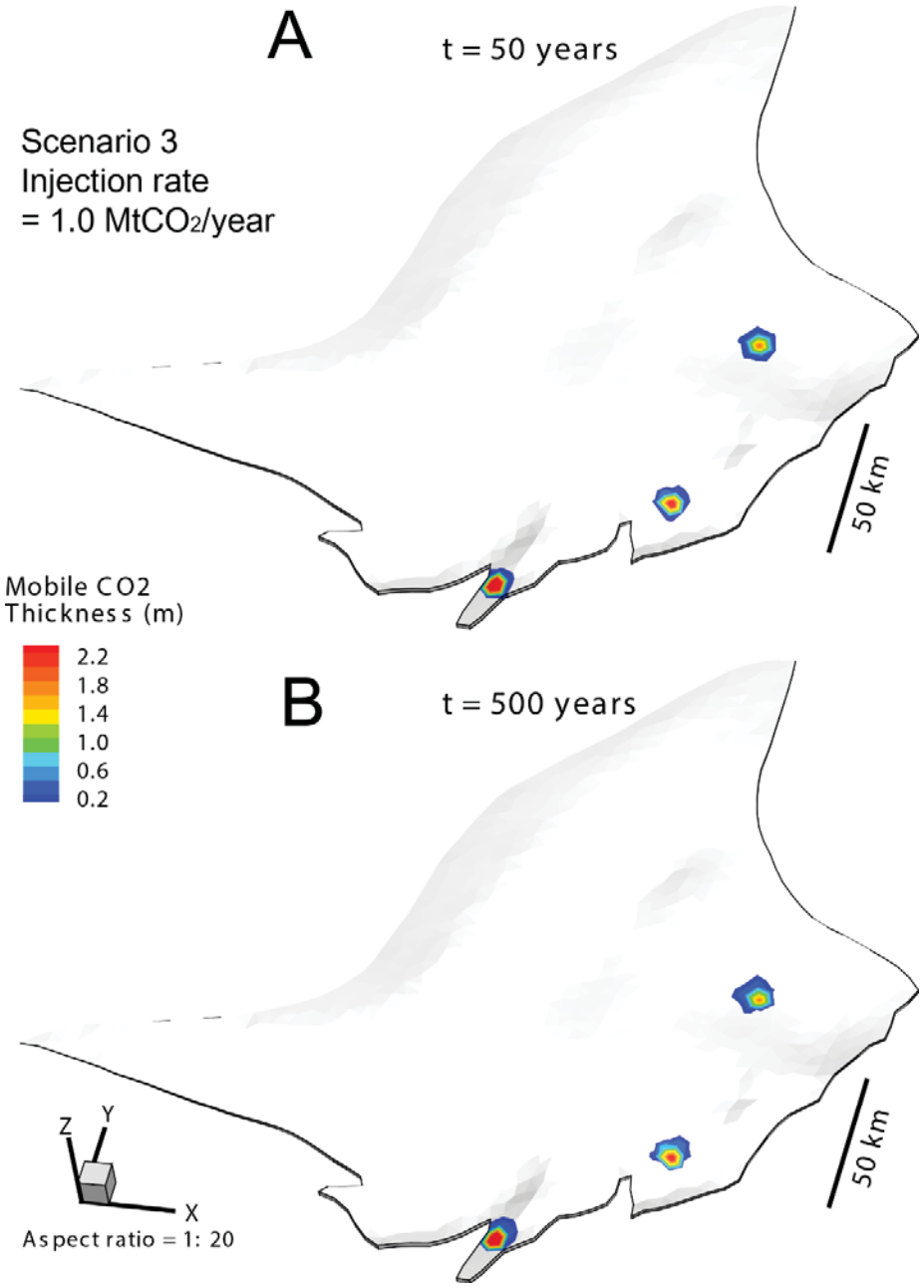

Figure 8. Scenario 3 - Mobile CO2 plume migration by the single-well CO2 injection with the rate of 1.0 Mt CO2/year per well for 50 years (Scenario 1). (a) 50 years after injection, (b) 500 years after injection (post-injection phase).

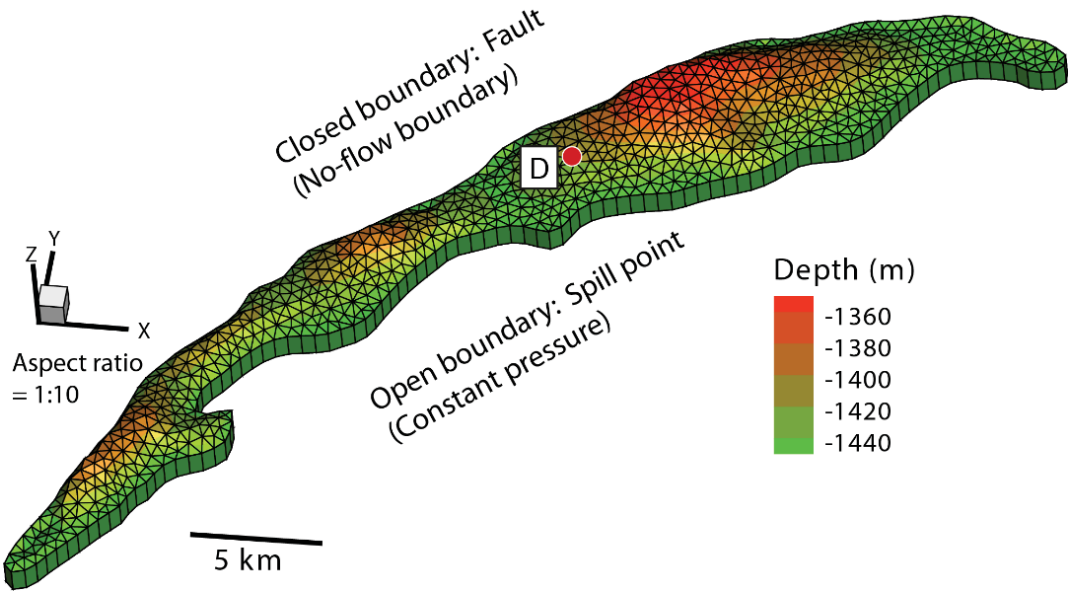

Figure 9. Numerical grid used in the dynamic modeling of the Dalders structure. The CO_2 injection well is marked by the red circle in the center of the structure.

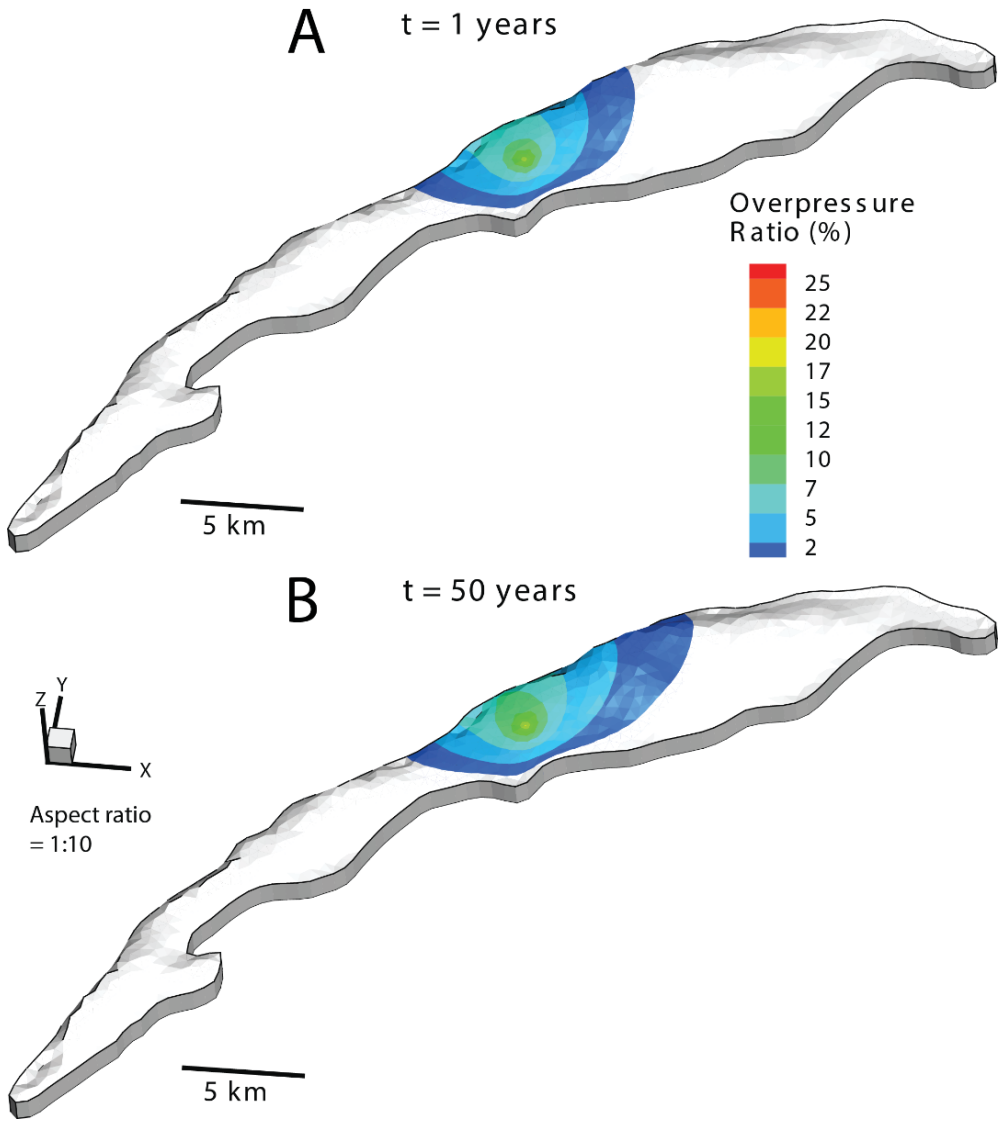

Figure 10. Overpressure ratio by the CO_2 injection with the rate of 0.3 Mt CO_2/year for 50 years. (a) 1 year after injection, (b) 50 years after injection.

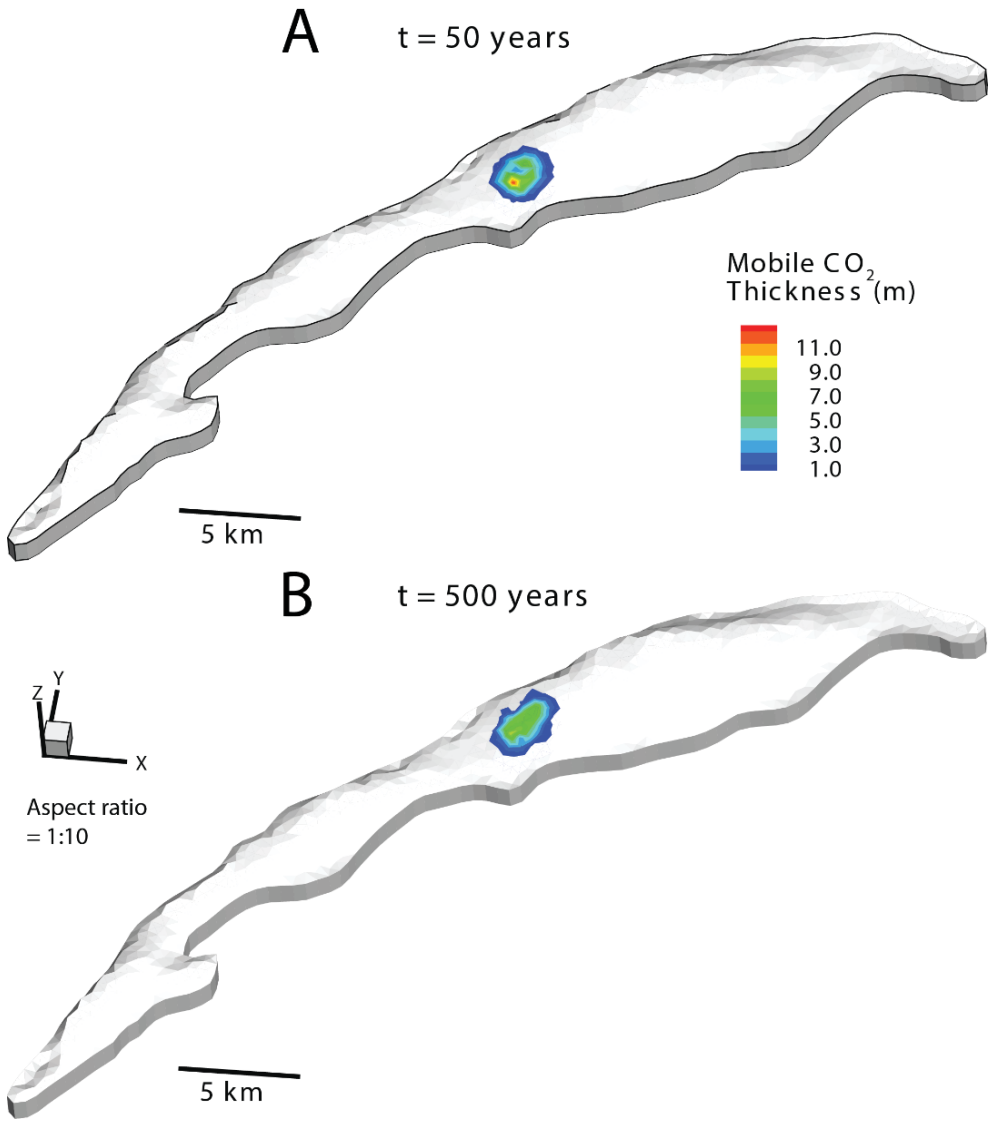

Figure 11. Mobile CO_2 plume migration by the CO_2 injection with the rate of 0.3 Mt CO_2/year for 50 years. (a) 50 years after injection, (b) 500 years after injection.

20.5 Conclusions

We have explored the effects of CO_2 injection in the submarine brine aquifers of Dalders Monocline and Dalders Structure, by modeling fluid pressure evolution and CO_2 plume migration during and after the injection. Three different injection scenarios varying the number of wells and injection rates were considered using the vertical equilibrium modeling approach. Based on the results, we can conclude the following:

1. With given hydrogeological parameters and an injection rate of 0.5 $MtCO_2$/year, the single-well injection could produce 70% ~ 80% overpressure ratio at the injection well after 50 years of injection.

2. The multiple-well injection could exacerbate overpressure evolution, and the location of the injection well is also shown to be important, in order to avoid high overpressures and potential risk of the caprock failure/fault reactivation. The injection well situated very close to the closed fault zone could induce an extreme overpressure of over 200% in the vicinity of the well.

3. Both 0.5 $MtCO_2$/year and 1.0 $MtCO_2$/year injection scenarios to the Dalders monocline create CO_2 plumes of less than 15 km with several meters thickness. The migration distance over 500 years is relatively small and insignificant considering the size of the monocline.

4. The 0.3 $MtCO_2$/year injection in the Dalders structure produced ~20% of overpressure and 3~4 km of CO_2 plume after 50 years of injection. The plume also shows a relatively strong topographically driven migration to the higher elevation area, driven by the buoyancy effect.

20.6 References

Bear J (1972) *Dynamics of Fluids in Porous Media*. Dover Publications, Inc., New York.

Gasda SE, Nordbotten JM, & Celia MA (2009) Vertical equilibrium with sub-scale analytical methods for geological CO_2 sequestration. *Computational Geosciences* **13**, 469-481, doi:10.1007/s20596-009-9138-x.

Gasda SE, Nordbotten JM, & Celia MA (2012) Application of simplified models to CO_2 migration and immobilization in large-scale geological systems. *International Journal of Greenhouse Gas Control* **9**, 72-84, doi:10.1016/j.ijggc.2012.03.001.

Gasda SE, Nilsen HM, Dahle HK, & Gray WG (2012) Effective models for CO_2 migration in geological systems with varying topography. *Water Resources Research* **48**, W10546, doi:10.1029/2012WR012264.

Gray WG, Herrera PA, Gasda SE, & Dahle HK (2012) Derivation of vertical equilibrium models for CO_2 migration from pore scale equations. *International Journals of Numerical Analysis and Modeling* **9**, 745-776.

Juanes R, MacMinn CW, & Szulczewski ML (2010) The footprint of the CO_2 plume during carbon dioxide storage in saline aquifers: storage efficiency for capillary trapping at the basin scale. *Transport Porous Media* **82**, 19-30, doi:10.1007/s11242-009-9420-3.

Szulczewski M & Juanes R (2009) A simple but rigorous model for calculating CO_2 storage capacity in deep saline aquifers at the basin scale. *Energy Procedia* **1**, 3307-3314, doi:10.1016/j.egypro.2009.02.117.

PART E

21.0 ESTIMATING CO_2 PLUME MIGRATION SPEED AND DISTANCE IN THE UP-DIP DIRECTION

Zhibing Yang, Saba Joodaki and Auli Niemi

Supercritical CO_2 injected into the Dalders monocline can migrate mainly in the up-dip direction below the cap-rock (an Alum shale layer), due to the gravity force (i.e., the density difference between brine and supercritical CO_2). This post-injection migration may constitute a concern of leakage risk e.g. at the Gotland island which is about 120 km away from a potential injection point. In order to evaluate the possibility of CO_2 plume reaching Gotland, we perform numerical simulations and analysis to address this issue based on all the available geological information.

21.1 Scenario

Since the CO_2 migration will be dominated by the sliding motion along the slope at large times, we consider a two-dimensional scenario (Figure 1) for investigating the potential of CO_2 up-dip migration. In this scenario, we cut a 2D vertical slice (1 m width) along the slope. Note that this is conservative in terms of CO_2 migration potential, as we ignore the expansion of CO_2 to direction other than the up-dip direction.

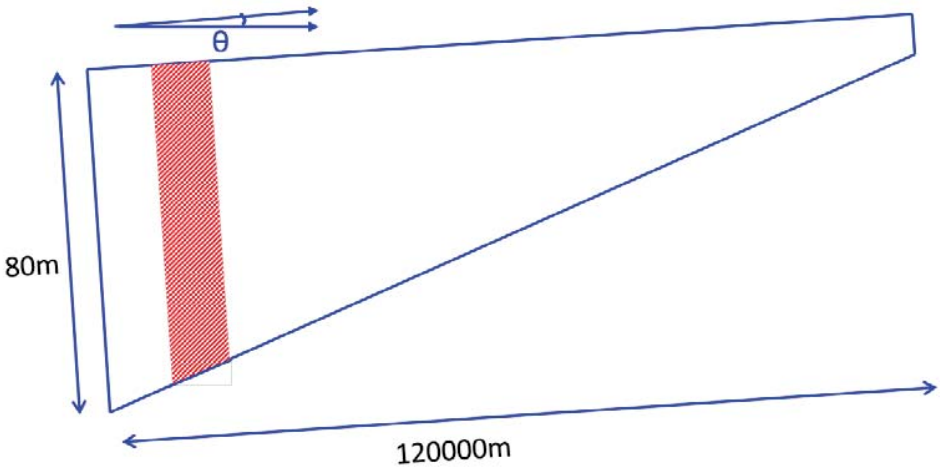

Figure 1. Schematic for the two-dimensional scenario considered in this study. The shadowed part shows the initial CO_2 plume placed in the domain

We use TOUGH2/ECO2N to simulate the migration of CO_2 in the formation. The simulation domain is discretized into 5540 grid blocks. We use a one-meter slice of the aquifer with an initial CO_2 plume of 1 km width. The initial plume is place at x = 14~15 km. The simulation results can provide CO_2 migration patterns and plume tip migration velocities.

The parameters used for the simulations are taken as the best estimates from the available information for the aquifer (Middle Cambrian sandstone). The slope of the aquifer is 0.5 degrees. The initial CO_2 plume depth is set as 1200 m. We test two different permeabilities: 30 and 100 mD, corresponding to the most probably range of permeability values. The thickness of the aquifer varies from 80 m at the deeper end of the aquifer to 5 meters at the shallower end of the aquifer. The porosity of the formation is assumed to be uniformly 0.1.

Capillary pressure and relative permeability functions are based on the Brooks-Corey function with parameter $\lambda = 0.670$, residual brine saturation $S_{lr} = 0.3$. We consider three different residual gas (CO_2) saturation values $S_{gr} = 0.1$, 0.2 and 0.3 to investigate parameter sensitivity. According to the measurement of residual CO_2 saturation for four different sandstones by Krevor et al. (2012), the more realistic values of S_{gr} would be in fact above 0.2 or even 0.3.

21.2 Simulation results

21.2.1 CO_2 saturation patterns

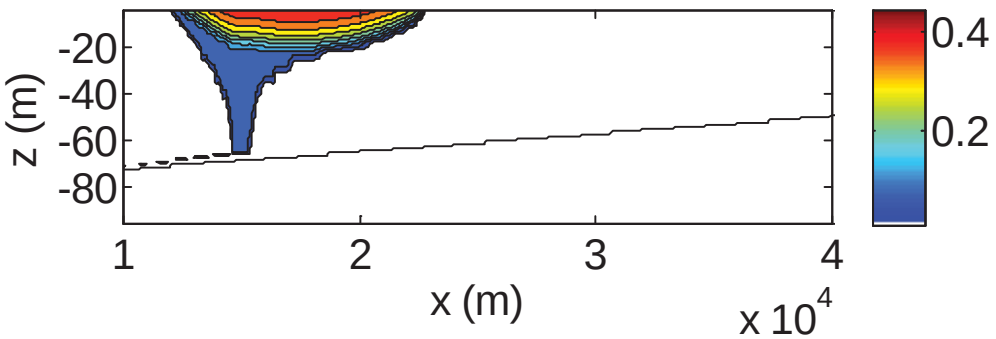

Figure 2. Simulated CO_2 saturation for the case of k=30 mD, residual CO_2 saturation 0.1, at time 2000 years.

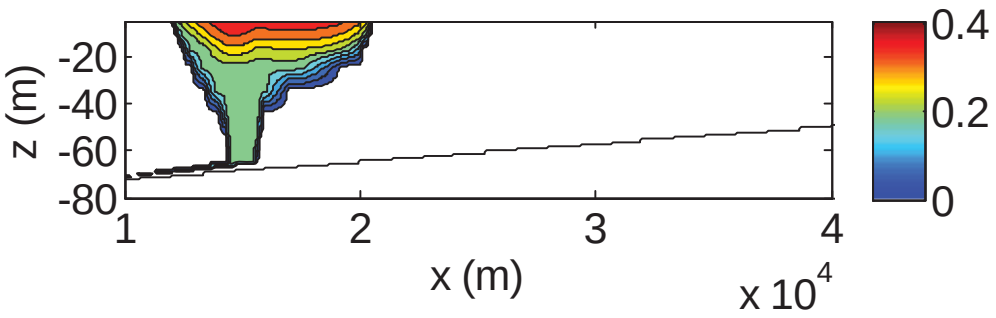

Figure 3. Simulated CO_2 saturation for the case of k=30 mD, residual CO_2 saturation 0.2, at time 3000 years.

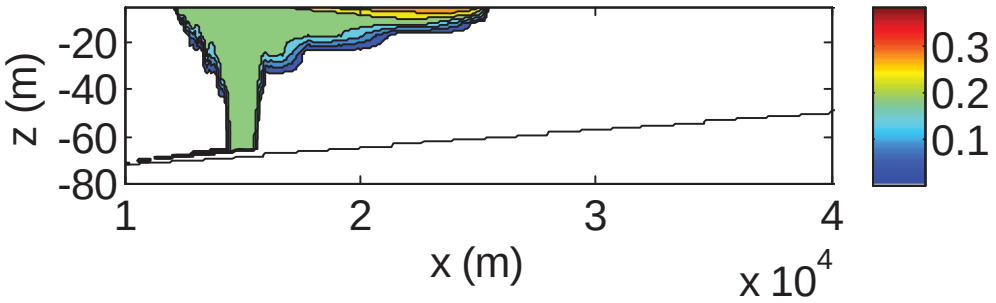

Figure 4. Simulated CO_2 saturation for the case of k=100 mD, residual CO_2 saturation 0.2, at time 2000 years.

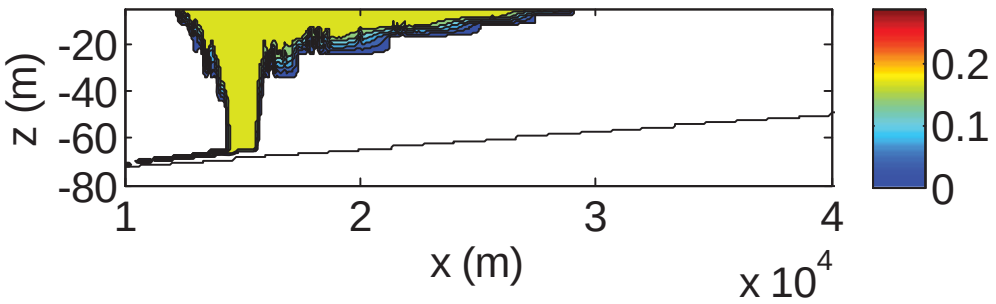

Figure 5. Simulated CO_2 saturation for the case of k=100 mD, residual CO_2 saturation 0.2, at time 4000 years.

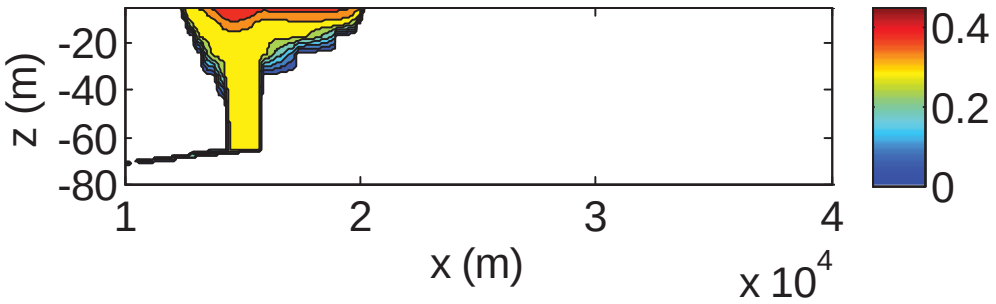

Figure 6. Simulated CO_2 saturation for the case of k=100 mD, residual CO_2 saturation 0.3, at time 2000 years.

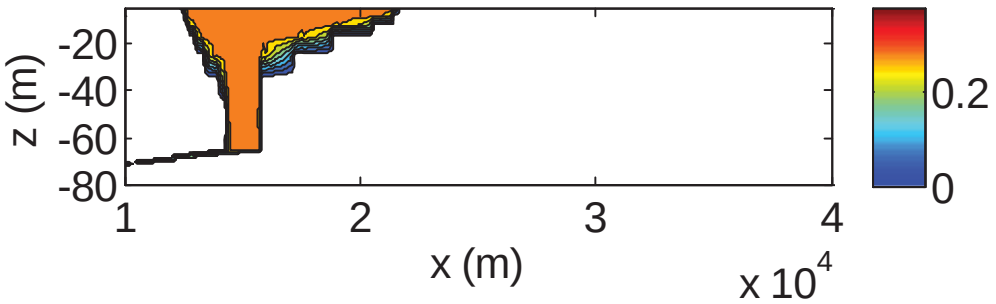

Figure 7. Simulated CO_2 saturation for the case of k=100 mD, residual CO_2 saturation 0.3, at time 4000 years.

Figures 2-7 show some of the simulated CO_2 saturation patterns at different (large) times for different permeabilities and residual gas saturations. It can be seen that the plume extends in the sloping direction and its thickness at the tip gradually decrease as the tip travels farther. These patterns all show the dependence of plume migration on the main parameters (formation permeability and residual gas saturation).

The CO_2 plume in these figures can be divided into two parts: the mobile part where CO_2 saturation $S_g > S_{gr}$ and the trapped (immobile) part where $S_g \leq S_{gr}$. The mobile CO_2 keeps migrating in the up-dip direction until all CO_2 becomes trapped as residual or dissolves in to the brine. For example, in the case of k= 100 mD and S_{gr} = 0.2, all mobile CO_2 has depleted and the migration has stopped after 4000 years. The plume tip has migrated about 14 km.

From Figures 2-7, we can see that plume thickness decreases from about 30 m just outside of the initial plume region to 0 m at the plume tip, for the scenario considered here. We note that the thickness of plume depends on the system parameters, especially the injected CO_2 volume. As a first order estimate, we may simply calculate an average thickness for the extended plume (excluding the initial plume zone) to be 15 m. With this average plume thickness and the residual

gas saturation, we can roughly estimate the volume of the CO_2 'footprint' and thus the plume tip distance if given a total CO_2 volume.

21.2.2 Plume tip migration distance and velocity

Parameters that can affect the migration of CO_2 plume in a sloping aquifer mainly include: permeability (and its anisotropy), residual CO_2 saturation, relative permeability of CO_2, slope, density difference between CO_2 and brine, CO_2 viscosity, etc. For the scenario considered in this study, the two most important parameters which are uncertain are the permeability and the residual gas saturation of the aquifer material.

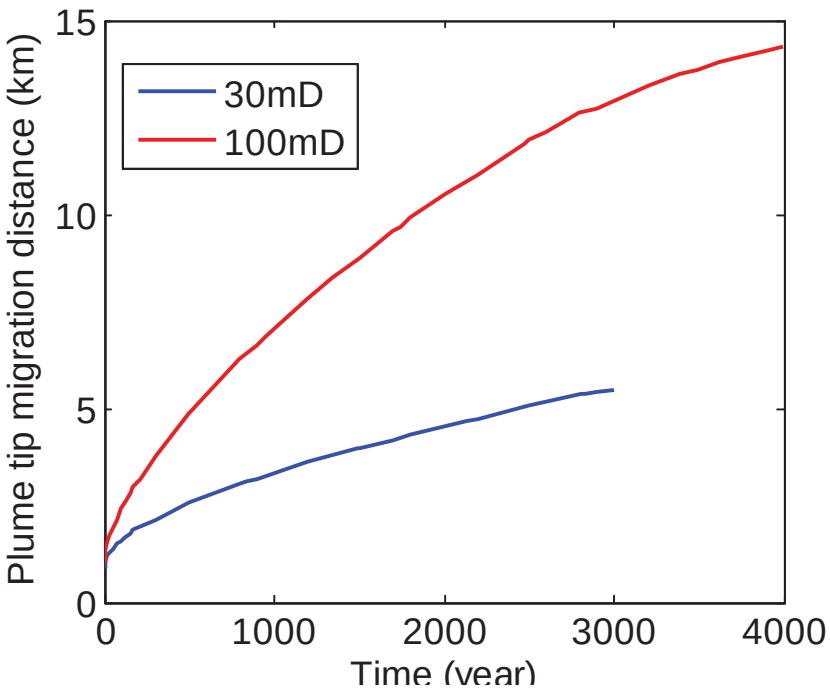

Figure 8. CO_2 plume tip migration distance as a function of time for permeabilities 30 and 100 mD. Residual gas saturation is 0.2 for both cases.

Figure 8 shows that permeability significantly affects the tip migration velocity. When k = 100 mD the plume tip migrated about 14 km in 4000 years, while for the case of k = 30 mD, the tip migrated less than 6 km in 3000 years.

Residual gas saturation has a large impact on the migration of CO_2 plume. As shown in Figure 9, increasing S_{gr} can greatly decrease the tip migration speed and the maximum migration distance. The plume tip has migrated less than 7 km in 4000 years when S_{gr} = 0.3, in comparison to 14 km when S_{gr} = 0.2. In the case of S_{gr} = 0.1, the plume tip migrates much faster, reaching 14 km in about

1250 years. However, 0.1 may be an unrealistically low value for residual gas saturation, given the measurements of typical sandstones relevant for CO2 storage by Krevor et al. (2012).

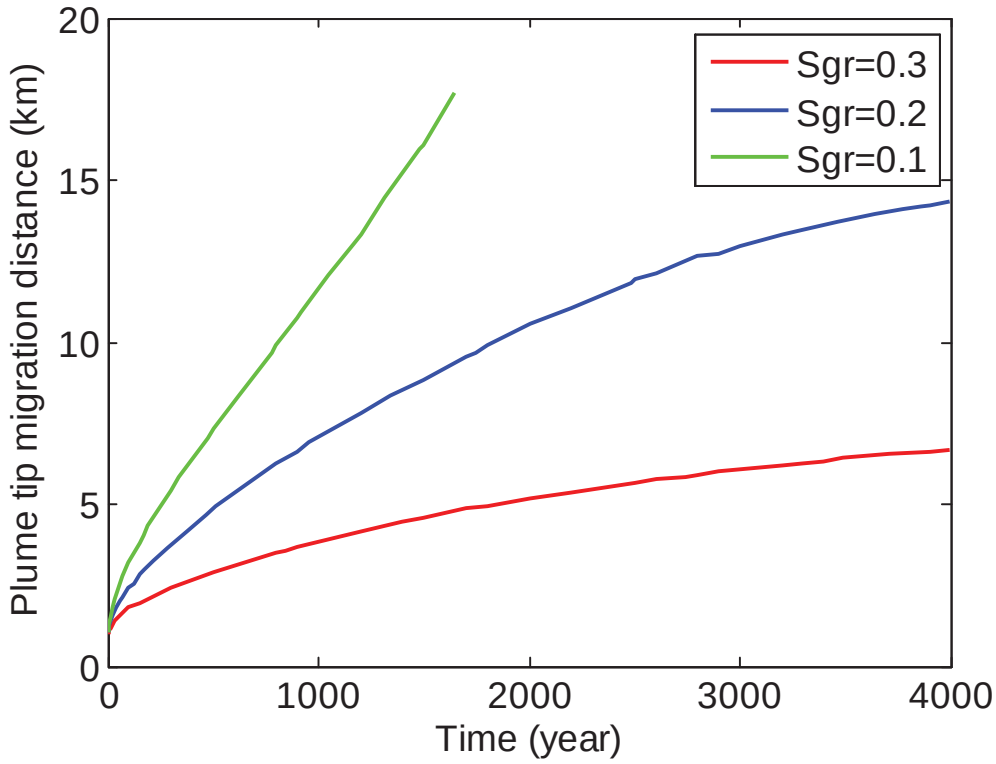

Figure 9. CO_2 plume tip distance as a function of time for different residual gas saturation values. Permeability k = 100 mD.

21.3 Discussion and conclusions

In the above simulations we have not included the effect of caprock topographic roughness (undulation) and the effect of convective mixing (or convective dissolution). Besides, in this 2D analysis, the expansion of the plume to outside of the 2D plane is not taken into account, which will slow down the migration and at the same time decrease the migration distance, especially in the case considered here with a slope of only 0.5 degree for the Monocline. Therefore, the analysis on the plume migration potential is conservative (i.e., the distance will be larger than the actual in the field).

The 2D scenario here can be thought of as a one-meter slice in the middle of the injected CO_2 cylindrical plume in a 3D view. In this 3D perspective, the scenario may correspond to about 3 Mt CO_2 for the injection point. According to the above results, the plume tip will migrate a maximum

distance of about 14 km and come to a stop within 4000 years, for the case of k = 100 mD and S_{gr}= 0.2. Again, these two important parameters are chosen to be conservative.

If we instead consider 30 Mt injected CO_2 for one injection point (well), this corresponds to an initial CO_2 mass of about 1.7×10^7 kg in the 2D scenario. If S_{gr}= 0.2, a simple volumetric calculation may yield a potential maximum migration distance of about 50 km, taking into account the plume shape (with average thickness for the part of plume extending to direction of the slope assumed to 15 m) and equilibrium dissolution within the plume. According to the average speed of migration (3.5 km/1000 year, which may be obtained from Figure 9) a migration distance of 50 km would take about 14000 years. Given this distance and the especially long time, we can also calculate the dissolution trapping capacity of this 2D slice aquifer, i.e., assuming convective mixing to reach its full effect. The mass that can potentially be dissolved in our considered system (50 km long 2D slice) is about 9×10^6 kg, which is more than half of the initial CO_2 mass. This means that, in this case, convective dissolution has the potential to significantly drag the plume migration, and that the plume migration distance will be actually much smaller than 50 km.

21.4 References

Krevor SCM, Pini R, Zuo L, & Benson AM (2012) Relative permeability and trapping of CO_2 and water in sandstone rocks at reservoir conditions. *Water Resour. Res.* **48**, W02532, doi:10.1029/2011WR010859.

Additional Note on Capillary Pressure and Relative Permeability Functions

The different models used in the previous chapters used different assumptions and thereby the treatment of so-called characteristic functions for the two-phase flow are treated differently in the different models. To allow the reader an easy comparison, we explain the use of these functions in the three models here

Capillary pressure functions

In the semi-analytical model for pressure buildup and in the vertical equilibrium (VE) numerical model, capillary pressure is ignored. Capillary pressure would have negligible impact on the pressure buildup (Mathias et al. 2011, WRR 47, W12525). Neglecting capillary pressure in the VE numerical model is justified as the VE model is a a much simpler model than the full-physics TOUGH2 model and the advantage of the VE model is its numerical efficiency.

Capillary pressure functions are only used in the TOUGH2 simulations. Because of a lack of experimental data on two-phase flow properties of the formation rock, we have assumed that the capillary pressure is a van Genuchten function with typical literature parameter values of m=0.457 and S_{wr} = 0.3. Parameters in the similar range have also been used in, e.g., Doughty (1997, Energy Conversion and Management, 48, 1768-1681) and Zhou et al. (Ground Water, 2010, 494-514).

Relative permeability functions

In the VE model, the saturation within the CO_2 occupied region is assumed to be constant (full gas saturation in this case). Thus relative permeability effects are not really taken into account. Through a vertical integration procedure, one can see that the vertical averaged relative permeabilities (pseudo-relative permeabilities) are linear functions of the thickness of the CO2 plume.

Again, in the TOUGH2 simulations we have to use the literature values of the relative permeability functions due to the lack of data.

Using the analytical model presented in Chapter 17, we can evaluate the impact of relative permeability parameters used on injection overpressure. A comparison of relative permeability functions used in the semi-analytical model for pressure buildup and in the TOUGH2 simulations is presented in Figure 1 below. It can be seen that there is notable differences between the two sets

of curves. However, the pressure buildup difference due to the different relative permeability functions is small (Figure 2 below, that can be compared to figures in the appendix A (Chapter 17) of the report).

Nevertheless, it would have been beneficial for modeling if more field data and core measurements especially regarding two-phase flow properties could be obtained. This is one of major sources of uncertainty. In future modeling work, we will refine the analysis by taken into account the uncertainty in the capillary pressure and relative permeability functions.

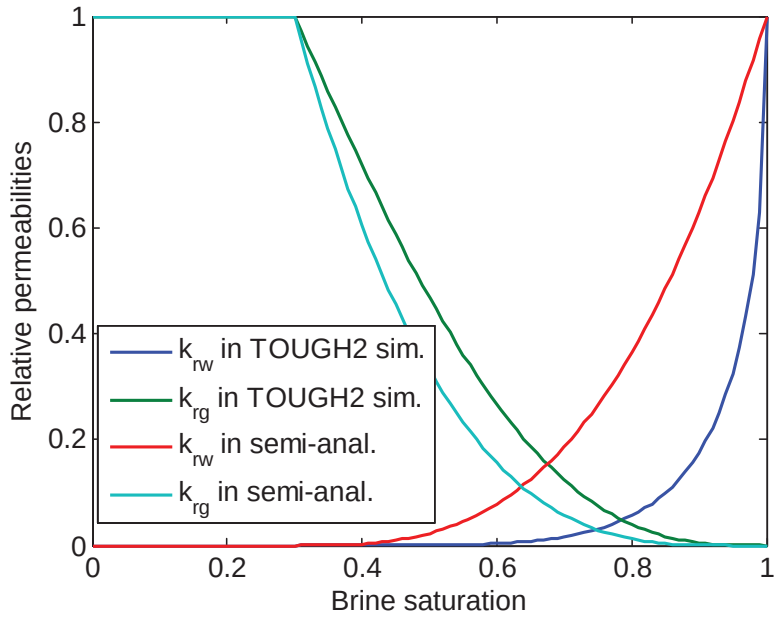

Figure 1. Relative permeability functions used in the semi-analytical model for pressure buildup and in the TOUGH2 simulations.

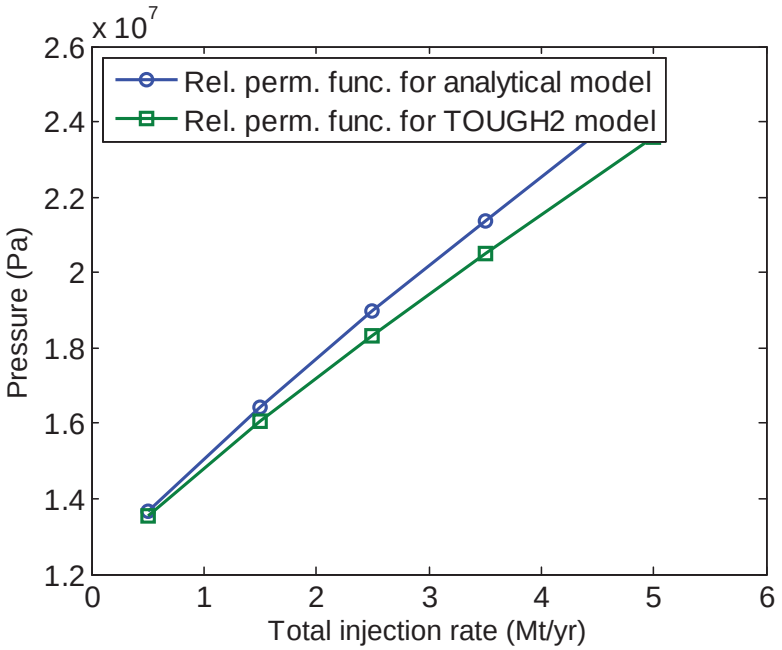

Figure 2. Comparison of pressure buildup from the semi-analytical model with two different sets of relative permeability functions from Figure 1.

Doughty, C. (2007), Modeling geologic storage of carbon dioxide: Comparison of non-hysteretic and hysteretic characteristic curves, *Energy Convers. Manag.*, *48*(6), 1768–1781.

Mathias SA, González Martínez de Miguel GJ, Thatcher KE, & Zimmerman RW (2011) Pressure buildup during CO_2 injection into a closed brine aquifer. *Transport in Porous Media* **89**, 383–97.

Zhou, Q., J. T. Birkholzer, E. Mehnert, Y.-F. Lin, and K. Zhang (2010), Modeling Basin- and Plume-Scale Processes of CO2 Storage for Full-Scale Deployment, *Ground Water*, *48*(4), 494–514.

ELFORSK

SVENSKA ELFÖRETAGENS FORSKNINGS- OCH UTVECKLINGS - ELFORSK - AB

Elforsk AB, 101 53 Stockholm. Besöksadress: Olof Palmes Gata 31
Telefon: 08-677 25 30, Telefax: 08-677 25 35
www.elforsk.se